Eidgenössische Technische Hochschule Zürich
Swiss Federal Institute of Technology Zurich

Bias in error-corrected quantum sensing

Master's Thesis

Ivan Rojkov
irojkov@ethz.ch

Trapped Ion Quantum Information group
Department of Physics, D-PHYS
ETH Zürich

Supervisors:
Dr. Florentin Reiter
Prof. Dr. Jonathan Home

December 7, 2020

Abstract

The sensitivity afforded by quantum sensors is often limited by decoherence. Quantum error correction (QEC) can enhance sensitivity by suppressing decoherence, but it has a side-effect: it biases the sensor's output in realistic settings. If unaccounted for, this bias systematically reduces the sensor's performance in experiment, and also give misleading values for the sensitivity in theory. This thesis analyzes this effect in the setting of continuous-time QEC, showing both how one can account for it, and how incorrect results can arise when one does not.

I would like to thank Dr. Florentin Reiter and Prof. Dr. Jonathan Home for the opportunity to conduct this master thesis following a semester project within the TIQI[i] group, introducing me to theory domains within the experimental world. Thank you as well for the numerous motivational and valuable remarks and advice.

I want to thank Dr. David Layden and Prof. Dr. Paola Cappellaro from MIT[ii] with whom I have collaborated for this work and who brought significant comments and suggestions during constuctive discussions. A special thank you to David for his initial contribution to the discrete quantum error correction model that I present in Section 2.2.

I am grateful to all members of the TIQI group for the many fruitful discussions and for the friendly atmosphere within the group. In particular, I would like to thank the members of the theory subgroup which have repeatedly listened to this topic during our weekly theory meeting. Moreover, I want to thank Maciej Malinowski who found the right words to explain the increase of the bias for weak corrections.

Last, but certainly not least, nothing would be possible without my beloved flatmates who encouraged me during these extraordinary times and contributed with beneficial questions, talks and advice. A special thank you to David Roschewitz for proof-reading my works and providing helpful comments.

[i] Trapped Ion Quantum Information
[ii] Massachussets Institute of Technology

Contents

Chapter 1

Introduction

Curiosity has always been a driving force for Humans to expand our understanding of nature by observing it. Indeed, scientific theories are built upon peoples' current perceptions of the world and these theories are then invalidated by new ones shaped by new observations. This process is known as scientific revolution. A perfect example of it is the development of our knowledge about gravity. From Copernicus who proposed a heliocentric model of the solar system up to Einstein's theory of general relativity, including Kepler's, Galileo's and Newton's works; all of them were made possible thanks to better observational techniques and devices.

Quantum mechanics has also derived from new physical observations such as the photoelectric effect monitored by Hertz in 1887 [1] and Gerlach's and Stern's experiment from 1922 [2], to mention just a few. These measurements gave rise to the development of quantum science and technologies. These in turn have led to the emergence of a wide range of new detectors that we now refer to as the first generation of quantum sensors. Photomultiplier tubes, atomic clocks, and semiconductor detectors are some examples of them. This first generation produced more precise observations than its classical predecessors and helped to validate some of the current physical theories such as the standard model of particle physics.

Over the past decades, new types of quantum sensors have generated a growing interest in the research community. In contrast to the first generation of quantum sensors which utilized the consequences of quantum effects, these detectors have the particularity of having quantized energy levels and using some direct quantum effects like coherence and entanglement. Usually referred to as "second generation quantum sensors" or "quantum-enhanced sensing"[3–5], they promise to have a better sensitivity than those from the first generation. They are now playing a part in major scientific advances as in the Laser Interferometer Gravitational Wave Observatory (LIGO) [6].

1.1. Quantum sensing

In this work, quantum sensors will be considered as belonging to this second generation. As mentioned above, they directly depend on quantum systems and effects. In particular, we consider that these quantum sensors satisfy the four criteria stated by Degen, Reinhard, and Cappellaro [7], mainly they are made of systems which:

1. Have discrete and resolvable energy levels. These are often restricted to only two (denoted by $|0\rangle$ and $|1\rangle$) in which case we speak of qubits.

2. Can be initialized in a fiducial state and we can read out their state.
3. Can be manipulated coherently.
4. Are able to interact with their environment and in particular with a relevant physical quantity $V(t)$.

Relevant physical quantities, as mentioned in point four, can range from the most common ones such as electro-magnetic fields up to temperature or pressure which have been less studied by the quantum sensing community. It is worth mentioning that the choice of parameters to detect is directly linked to the type of quantum system. Indeed, each physical system is more sensitive to some particular signals than others; for instance trapped ions are more suitable for sensing electric and magnetic fields, whereas optomechanical systems are appropriate for measuring forces and accelerations.

Finally, a crucial part of any quantum detector is the sensing protocol, which consists of a sequence of operations that result in measurements of the desired quantity $V(t)$. It can often be divided into three steps: initialization, interaction and read out [7]. These can be linked to the steps of quantum computing protocols. The first and last steps remain identical, whereas the intermediate phase, responsible for the acquisition of information about $V(t)$, can be seen as the processing step. The two most common protocols are Ramsey interferometry and Rabi measurement. In this work, we will focus on the former which will be presented in greater detail in the next chapter. However, conclusions drawn in the following chapters will also concern other sensing protocols as long as required assumptions are fulfilled.

A key criterion characterizing the efficiency of a sensor is its sensitivity. It is defined as the minimum detectable signal per unit time, which, put in other words, means the minimal variation $\delta V(t)$ that leads to a unit signal-to-noise ratio (SNR). An ideal sensor would thus be a device which gives an infinite response to fluctuations of the quantity to sense and, at the same time, remains robust to undesirable input signals. However, quantum systems are intrinsically susceptible to any type of disturbances induced by their environment. It is thus challenging to make them sensitive to the desired signal and at the same time robust against unwanted noise and decoherence. The competition between these two contributions is what fundamentally limits the sensitivity of a quantum sensor[i].

1.2. Quantum error correction

One method to limit effects of noise and decoherence on a quantum system is to make use of so-called quantum error correction (QEC). Like its classical counterpart, it rests on two elements: detection of errors and their correction. While classical error correction used in classical computation relies largely on the redundancy of information (e.g. in a repetition code), QEC cannot due to three natural obstacles [8]:

(a) The no-cloning theorem forbids duplication of quantum information.

[i]We do not consider initialization and manipulation errors which could potentially be fully eliminated.

(b) Errors in quantum systems are not discrete processes but occur in a continuous manner.

(c) Every read-out of the system's state destroys it together with the quantum information it retains.

A way to overcome these restrictions is to use a specific encoding for representing the two quantum states of a qubit. We will refer to them as logical quantum states denoted by $|0\rangle_L$ and $|1\rangle_L$. The first proposal of such encoding was made by Shor [9] in 1995. One of Shor's main contributions was to encode one logical qubit using N physical ones in the following way : $|0\rangle_L = |0\rangle^{\otimes N}$ and $|1\rangle_L = |1\rangle^{\otimes N}$. This code can be seen as the quantum variant of the classical error correction mentioned above since in both cases the detection of errors is performed via majority vote, i.e. information held by the majority of the qubits prevail. There is however a fine distinction between both implementations: in the quantum case, information is not processed by one instance and then copied onto several qubits, but rather embodied by many two-level systems and processed using logical operations implemented collectively. We will refer to this encoding as (quantum) repetition code.

Immediately following Shor's proposal, a variety of new encodings were suggested such as the seven qubit code by Steane [10]. In this work, we will nevertheless focus only on a simple three-qubit code that will be explained in more detail in the next chapter.

1.3. Error-corrected quantum sensing

As mentioned above, QEC is one technique which allows to filter out the decoherence noise. It can be applied in quantum sensing to eliminate the unwanted noise and thus to increase the SNR. However, the major restriction of error-corrected quantum sensing comes from the fact that one cannot use QEC to correct all types of errors. Since the crucial part of a sensing protocol is to sense $V(t)$, we are restricted to correct for errors perpendicular to the signal, otherwise we would unintentionally deteriorate the information about the signal[ii]. Although experimentally $V(t)$ and decoherence noise often couple to the system through the same operators [12–17], one can engineer some systems which could be used for error-corrected quantum sensing. On this basis, various QEC schemes have already been proposed for sensing purposes [18–26] and two experimental implementations [27, 28] have been realized. The latter have shown that QEC enhances the sensing time of the protocol but do not exhibit any significant improvement of its sensitivity.

Another techniques for filtering out the decoherence noise in a quantum system is the so-called dynamical decoupling (DD). While being widely used in quantum sensing [29–36], it presents some disadvantages, like its inability to directly sense DC signals or its dependence on the noise frequency [37]. Error-corrected quantum sensing is not

[ii] This condition is thoroughly studied in the PhD thesis of David Layden [11] and it turns out to be in general wrong. In this thesis, we will however assume only errors perpendicular to the signal.

affected by these limitations which makes it a preferable technique to DD[iii]. The noise and error-correction models chosen for this work will be presented in the next chapter.

[iii]DD can nevertheless be useful in other situations than QEC, e.g. fast coherent noise.

Chapter 2

Model

2.1. Continuous model

One of the four criteria that a quantum sensor has to satisfy, mentioned in Section 1.1, is the ability to interact with a relevant physical quantity $V(t)$. This mathematically means that there exists a Hamiltonian which couples the qubit to the signal to sense [7]

$$H_V(t) = \xi\,\mathrm{Re}[V_\perp(t)]\,\sigma_x + \xi\,\mathrm{Im}[V_\perp(t)]\,\sigma_y + \xi\,V_\parallel(t)\,\sigma_z \tag{2.1}$$

where σ are the Pauli operators and ξ – the coupling constant[i]. Here $V(t)$ has been decomposed into a parallel component $V_\parallel(t)$ which affects the energy levels of the sensor and a perpendicular one $V_\perp(t)$ which can swap its state. Since the quantum sensor could be made of multiple qubits, the interaction of the sensor with the signal would be represented as the sum over all the qubits of Hamiltonians like the one given in Eq. (2.1).

For the sake of simplicity, we assume that the signal to sense is a direct current (DC), meaning $V(t) = V$. On top of that, we consider that it couples to the qubits of the system through the same operators as their transition energy ω_q, in other words the system's Hamiltonian can be written as following

$$H = \sum_j \frac{\omega_q}{2}\,\sigma_z^{(j)} + \xi V\,\sigma_z^{(j)} = \sum_j \frac{\omega}{2}\,\sigma_z^{(j)}\ , \tag{2.2}$$

where the j index refers to a particular qubit. The second equality synthesizes both the static and dynamic parts of the Hamiltonian in one parameter $\omega = \omega_q + 2\,\xi\,V$. The goal of a quantum sensing protocol is then to estimate the latter parameter. Throughout this work, we will refer to it as *(true) frequency* or just ω.

In order to utilize QEC for sensing one has to assume that the noise model is perpendicular to the signal to sense, otherwise one could corrupt the information accumulated within the sensor about V. Following Refs. [18, 20, 21, 25, 28], we assume that the noise is predominantly due to bit flips which in the Lindbladian framework are represented by the jump operators $L_{\mathrm{err}}^{(j)} = \sqrt{\Gamma_{\mathrm{err}}}\,\sigma_x^{(j)}$, with Γ_{err} being the rate at which bit flips occur. Lindblad dynamics, i.e. Markovian trace-preserving and completely positive master equations [38], represents a pessimistic noise model for quantum sensors. It thus describes noise devoid of the temporal correlations exploited by many noise-suppression schemes for sensing, such as dynamical decoupling. Note that we consider the qubits to

[i] Note that this work uses $\hbar = 1$

be identical which means that they have the same transition energy and error rate, as opposed to mixed species systems in Refs. [23, 24, 26, 27].

Correcting for single bit-flip errors requires the use of codewords of distance greater than or equal to two. We therefore choose to use a three-qubit repetition code, i.e., the codespace of interest is $\{|0\rangle_L, |1\rangle_L\} \equiv \{|000\rangle, |111\rangle\}$. We assume that quantum error detection and correction are implemented in a continuous dissipative manner using the following jump operators [25]

$$, L_{\mathrm{qec}}^{(j)} = \sqrt{\Gamma_{\mathrm{qec}}}\, \sigma_x^{(j)}\, \frac{1-\sigma_z^{(j)}\,\sigma_z^{(k)}}{2}\, \frac{1-\sigma_z^{(j)}\,\sigma_z^{(l)}}{2}\ , \tag{2.3}$$

with $j, k, l \in \{1, 2, 3\}$ such that all of them are different, and where the first index indicates which qubit is corrected. Moreover, the correction rate Γ_{qec} reflects the strength of the correction process (i.e. the transfer of erroneous states back into logical ones). This parameter can in principle be engineered [25]. Moreover, the operators given in Eq. (2.3) are constructed in a way such that the correction $\sigma_x^{(j)}$ is applied if and only if the parity of the j-th qubit is inverted with respect to the parity of the two other qubits.

It is worth to mention that often instead of considering $H \propto \sigma_z$ and $L_{\mathrm{err}} \propto \sigma_x$, some works looked at the problem from the opposite point of view by taking $H \propto \sigma_x$ and $L_{\mathrm{err}} \propto \sigma_z$. This only changes the codewords used by the sensing protocol but not the conclusions of our work since the signal and the noise remain perpendicular in both cases.

In the Lindbladian framework, the evolution of the system is given by the following master equation

$$\frac{\mathrm{d}}{\mathrm{d}t}\,\rho = -i\,[H,\,\rho] + \sum_j \mathcal{D}[\,L_{\mathrm{err}}^{(j)}\,](\rho) + \sum_j \mathcal{D}[\,L_{\mathrm{qec}}^{(j)}\,](\rho) \tag{2.4}$$

where ρ is the system's density matrix and $\mathcal{D}[\,L_k\,]$ represents the dissipator, a superoperator defined as

$$\mathcal{D}[\,L_k^{(j)}\,](\rho) := L_k^{(j)}\,\rho\,L_k^{(j)\,\dagger} - \frac{1}{2}\left(L_k^{(j)\,\dagger}L_k^{(j)}\,\rho\,+\,\rho\,L_k^{(j)\,\dagger}L_k^{(j)}\right) \tag{2.5}$$

where $L_k^{(j)}$ is a jump operator. The master equation given in Eq. (2.4) can be rewritten in a more reduced form using the so-called Liouvillian $\mathcal{L}$

$$\dot{\rho}(t) = \mathcal{L}\,\rho \qquad\qquad \text{where} \quad \mathcal{L} = -i\,\mathcal{H} + \tilde{\mathcal{D}}_{\mathrm{err}} + \tilde{\mathcal{D}}_{\mathrm{qec}}\ . \tag{2.6}$$

Here $\mathcal{H}$ denotes the superoperator responsible for the unitary evolution and $\tilde{\mathcal{D}}_{\mathrm{err}}$ and $\tilde{\mathcal{D}}_{\mathrm{qec}}$ are the system's dissipators for errors and QEC.

A typical quantum sensing protocol is standard Ramsey interferometry [39]. In our case it starts with initializing the system in the logical 0 state, applying a logical Hadamard transform which brings the state into the superposition $\frac{1}{\sqrt{2}}(|0\rangle_L + |1\rangle_L)$. In the quantum optics community, this step is sometimes referred to as Ramsey or $\pi/2$ pulse. Then the state evolves freely for a sensing time τ (also known as Ramsey time) according to the Liouvillian $\mathcal{L}$. The last two stages of the sequence are a second logical Hadamard transform and a measurement of the state's parity $\mathbb{P}_1 \equiv \langle 1|_L \, \rho \, |1\rangle_L$. Repeating the experiment for several runs and for different sensing times gives rise to an oscillating function $\mathbb{P}_1(\tau)$ that we will refer to as *parity function* or *parity signal*. The frequency of this signal will exactly correspond to the frequency ω that we aim to determine. An example of such a function is given in Fig. 3.1.

2.2. Discrete model

The dissipators (2.5) together with the jump operators given in Eq. (2.3) represent a continuous way to look at QEC with Γ_{qec} being the correction rate. We can also implement it in a discrete way, where QEC is performed by perfect quantum gates $\mathcal{R}$ which are applied every $\delta\tau$ time step (cf. Fig. 2.1). These gates then have the role of detection and correction of errors in the system. If such a procedure is repeated for c cycles and the gate time is assumed to be negligible, then the total free evolution period in the Ramsey experiment would be given by $\tau = c\,\delta\tau$. In-between QEC gates, the system evolves by a Lindblad equation $\dot{\rho} = \mathcal{L}\,\rho$ where the Liouvillian includes only the unitary evolution and the error dissipators, $\mathcal{L} = -i\,\mathcal{H} + \tilde{\mathcal{D}}_{\text{err}}$.

The system's evolution for a single cycle is given by $\mathcal{R}\,\mathrm{e}^{\mathcal{L}\delta\tau}$ and that of the entire sensing period is $(\mathcal{R}\,\mathrm{e}^{\mathcal{L}\delta\tau})^c$. Due to the complexity of this expression, it is convenient to describe the dynamics of the system through an effective Liouvillian $\mathcal{L}_{\text{eff}}$ defined as $\mathrm{e}^{\mathcal{L}_{\text{eff}}\delta\tau} = \mathcal{R}\,\mathrm{e}^{\mathcal{L}\delta\tau}$. The expansion on the latter in power series leads to the following expression for $\mathcal{L}_{\text{eff}}$,

$$\begin{aligned}
\mathcal{L}_{\text{eff}} &= \frac{1}{\delta\tau}\ln\left[\mathcal{R}\,\mathrm{e}^{\mathcal{L}\delta\tau}\right] = \frac{1}{\delta\tau}\ln\left[\mathbb{1} + \delta\tau\,\mathcal{R}\mathcal{L} + \frac{\delta\tau^2}{2!}\,\mathcal{R}\mathcal{L}^2 + \mathcal{O}(\delta\tau^3)\right] = \\
&= \mathcal{R}\mathcal{L} + \frac{\delta\tau}{2!}\,\mathcal{R}\mathcal{L}^2 - \frac{1}{\delta\tau}\frac{1}{2}\left[\delta\tau\,\mathcal{R}\mathcal{L} + \frac{\delta\tau^2}{2!}\,\mathcal{R}\mathcal{L}^2\right]^2 + \mathcal{O}(\delta\tau^3) = \\
&= \mathcal{L}_0 + \delta\tau\,\mathcal{L}_1 + \frac{\delta\tau^2}{2!}\,\mathcal{L}_2 + \dots\ ,
\end{aligned}$$

where:

$$\mathcal{L}_0 = \mathcal{R}\mathcal{L} \qquad \text{and} \qquad \mathcal{L}_1 = \frac{1}{2}\,\mathcal{R}\mathcal{L}^2 - (\mathcal{R}\mathcal{L})^2\ .$$

The main idea behind QEC is to correct the decoherence induced by the dissipator $\mathcal{D}$ and not the action of the Hamiltonian $\mathcal{H}$. This means in our case that the QEC superoperator $\mathcal{R}$ has the property that $\mathcal{R}\mathcal{D} \equiv 0$ and $\mathcal{R}\mathcal{H} \equiv \mathcal{H}_{\text{eff}}$ where the latter is the projection of H onto the logical subspace. This ensures that for $\delta\tau \to 0$ (i.e. continuous and ideal QEC), the effective dynamics becomes unitary and is generated by $\mathcal{L}_0 = -i\omega\mathcal{H}_{\text{eff}}$. The correction rate that was introduced in the previous section would then be inverse proportional to the QEC time step, i.e. $\Gamma_{\text{qec}} \propto (\delta\tau)^{-1}$, and thus the effective Liouvillian $\mathcal{L}_{\text{eff}}$ can be seen as the expansion of the continuous evolution (cf. Eq. (2.4)) in the regime of very good error-correction.

In this work, we decide to focus on exclusively the continuous evolution instead of the discrete one and will thus not go further in its derivation. We will however argue in Section 4.3 that the discrete point of view leads to the same effects and conclusions.

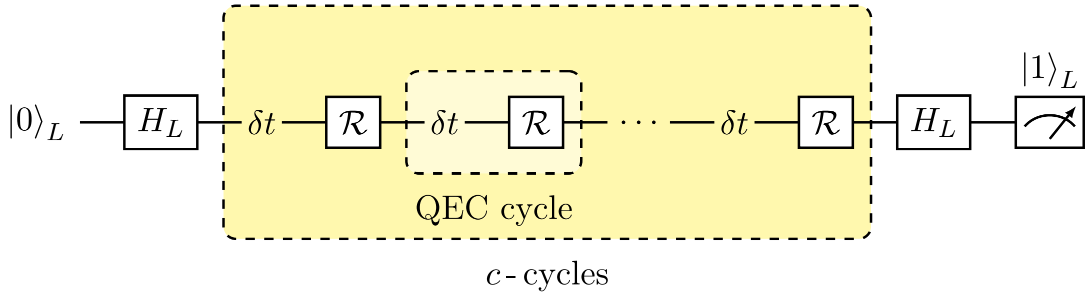

Figure 2.1.: *Error-corrected Ramsey sequence.* A quantum circuit representing the Ramsey sequence enhanced with quantum error correction (QEC). The H_L gates are the so-called Hadamard gates, whereas the $\mathcal{R}$ embody the detection and correction gates. One QEC cycle is constituted of a free evolution time δt as well as a $\mathcal{R}$ gate. The whole sequence is composed of c-cycles such that the total sensing time is $\tau = c\,\delta t$. The sequence concludes with a measurement of the system in the logical 1 state.

Chapter 3

Objective

3.1. Estimation problem

As we have discussed in the previous chapter, the goal of a Ramsey interferometry experiment is to assess the frequency of the parity signal $\mathbb{P}_1(\tau)$ which holds information about the signal to sense. The problem can then be restated as an estimation problem where we aim to find an estimator $\hat{\omega}$ of the frequency such that the expectation value of this quantity is equal to the true value ω plus eventually a bias $b(\omega)$:

$$\mathbb{E}[\,\hat{\omega}\,] = \omega + b(\omega) \ .$$

Since the bias corrupts the information about the frequency, we would like to either fully understand or entirely eliminate the bias, in which case we obtain an *unbiased estimator*.

In this work, we are using non-linear least squares regressions as estimators,

$$\hat{\omega} = \arg\min_{\omega} \sum_{\tau} \left[\, X_\tau - \mathbb{P}_1(\tau, \omega, \Gamma_{\text{err}}, \Gamma_{\text{qec}}) \,\right]^2 \ , \tag{3.1}$$

where X_τ are interferometry data points obtained experimentally or via a simulation. We allow here the parity function to also depend on the error rate Γ_{err} and on the correction rate Γ_{qec}. However, the problem is still considered as univariate, since these parameters remain constant during the minimization process. Moreover, due to the non-linearity of $\mathbb{P}_1$, Eq. (3.1) does not have a straightforward closed-form solution. Two distinct estimators will then differ in their accuracy only by the choice of the parity function. The motivation of this work is to show that some functions are better candidates for $\mathbb{P}_1$ in Eq. (3.1) than others.

3.2. Preliminary observations

Let us start with the previously proposed solutions for the parity function and some preliminary observations. First, we must consider the ideal noiseless situation. It is straightforward to see how the equal superposition state would unitarily evolve under the action of the Hamiltonian in Eq. (2.2). This unitary operator is given by $U(\tau) = \exp\left(-i\, H_s\, \tau\right)$

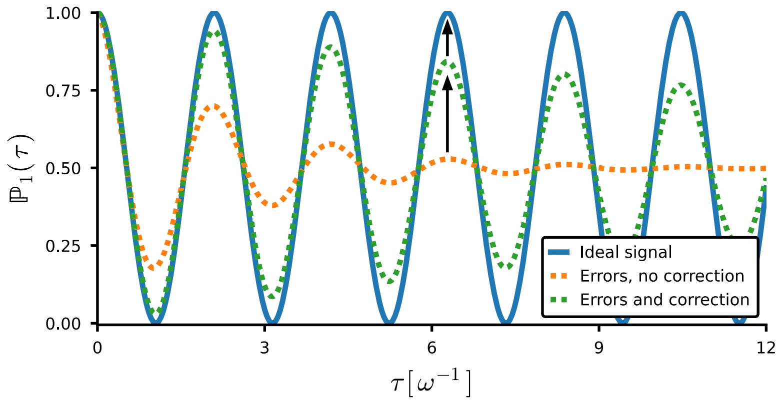

Figure 3.1.: *Expected parity functions.* The parity signal $\mathbb{P}_1$ as a function of the free evolution time τ for three different sensing models: ideal (blue), uncorrected (orange) and error-corrected (green). While the first plot is based on an actual calculation, the others are plotted from calculation explained in the main text. The arrows show the expected trend for increasing correction rate.

and the state evolution reads (up to a global phase) as

$$\frac{1}{\sqrt{2}}\left(|0\rangle_L + |1\rangle_L\right) \xrightarrow{U(\tau)} \frac{1}{\sqrt{2}}\left(|0\rangle_L + \mathrm{e}^{-i\,3\,\omega\,\tau}\,|1\rangle_L\right)\ . \tag{3.2}$$

After the second Hadamard transform, the state measurement in the logical 1 basis leads to the parity function

$$\mathbb{P}_1(\tau) = \frac{1}{2} + \frac{1}{2}\cos[3\,\omega\,\tau]\ . \tag{3.3}$$

In Fig. 3.1, this function is shown in blue.

However, this perfect parity signal gets damped in the presence of decoherence. In fact, with every bit flip, the information contained originally in the factor $\exp(-i\,3\,\omega\,\tau)$ in Eq. (3.2) is slowly damped by the noise over the course of the waiting time. Ultimately, if τ is long enough such that a sufficiently large number of quantum jumps has occurred during this sensing period, the state ends up in a equal superposition of $|0\rangle_L$ and $|1\rangle_L$. Thus, the function which represents the parity signal is expected to be

$$\mathbb{P}_1(\tau) = \frac{1}{2} + \frac{1}{2}\,\mathrm{e}^{-3\,\Gamma_{\mathrm{err}}\,\tau}\cos[\,3\,\omega\,\tau\,]\ . \tag{3.4}$$

Here the factor 3 in the damping exponential comes from the number of qubits in the system. This function is plotted in orange in Fig. 3.1. While Eq. (3.4) is, here, empirically inferred, it was first derived by Huelga, Macchiavello, Pellizzari, Ekert, Plenio, and Cirac [40] as an exact solution to a Ramsey experiment in the presence of phase-flip noise. Throughout this work, we will refer to this equation as the *well-established, canonical* or *standard* formula.

With the introduction of QEC into the system, we would naturally expect that the only element that gets modified in the previous equation is the damping term which would be attenuated and eventually, for an infinitely large correction rate $\Gamma_{\rm qec}$, would be driven to zero. This would mean that a good approximation to the parity function in this situation is

$$\mathbb{P}_1(\tau) = \frac{1}{2} + \frac{1}{2}\,\mathrm{e}^{-3\,\Gamma_{\rm eff}(\Gamma_{\rm err},\Gamma_{\rm qec})\,\tau}\,\cos[\,3\,\omega\,\tau\,]\;. \tag{3.5}$$

Here, $\Gamma_{\rm eff}$ denotes an effective decay rate and is a function of the error and correction rates. If Eq. (3.5) represents the true nature of the error-corrected signal, one can conclude that the estimator from Eq. (3.1) is unbiased since ω is a decoherence-independent variable.

The preliminary observations show, however, a different behavior. They are synthesized in Fig. 3.2. A summary of the error-corrected Ramsey protocol that has been explained in Section 2.1 can be seen in Fig. 3.2A. It shows simulations of Ramsey sequences in three different situations: the ideal one; a case with only errors and an error-corrected situation. These simulations were performed using the Quantum Toolbox in Python (QuTiP) [41]. From Fig. 3.2B, we observe a difference in the frequency of the ideal and the corrected parity signals, which we emphasize with the shaded areas. This points out the fact that the assumption of a decoherence independent frequency is seemingly wrong

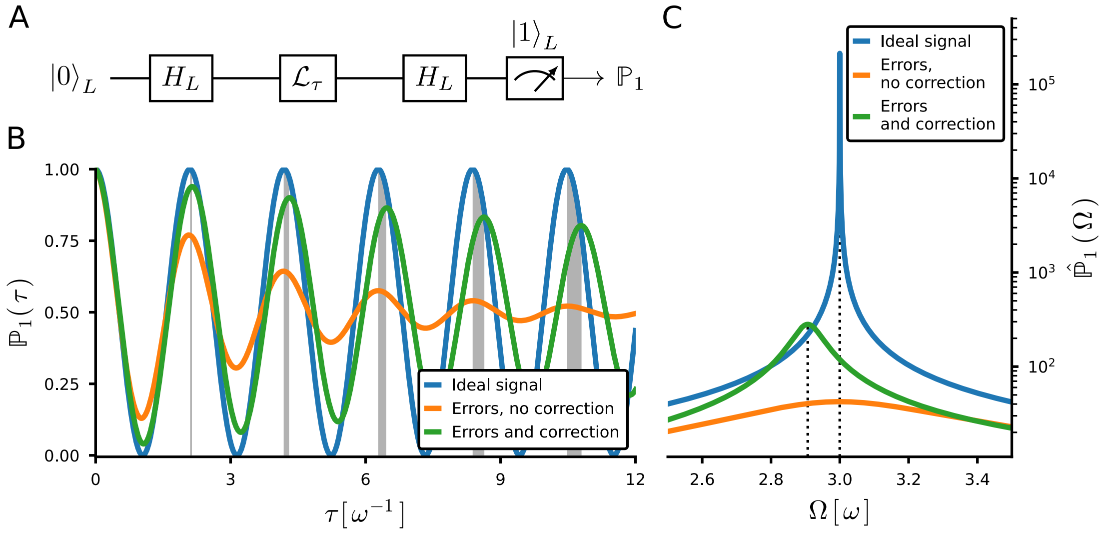

Figure 3.2.: *Overview of the preliminary observations.* **A.** Error-corrected Ramsey sequence represented as a quantum circuit where H_L is a logical Hadamard gate and $\mathcal{L}_\tau$ illustrates a free evolution of duration τ. **B.** The parity function $\mathbb{P}_1$ as a function of the free evolution time τ for three different sensing models: ideal, uncorrected and error-corrected. **C.** The Fourier transform of the parity functions from Fig. 3.2B denoted as $\hat{\mathbb{P}}_1(\Omega)$.

or at least that it depends nontrivially on the correction rate. This *bias* is even more pronounced on the Fourier transform plot showed in Fig. 3.2C. If we only had knowledge of the error-corrected curve and not the ideal case, the error on the frequency that we would obtain using Eq. (3.5) is approximately 3%. This would be a non-negligible error especially for sensors meant for precision metrology.

This shift in the frequency can also be observed in some previous works about error-corrected quantum sensing (cf. Fig. 2 in Arrad, Vinkler, Aharonov, and Retzker [21] or Fig. 6 in Reiter, Sørensen, Zoller, and Muschik [25]). Nevertheless, there exists neither a mathematical nor a physical explanation of this phenomenon in the literature. In the next two sections, we rewrite the master equation (cf. Eq. (2.4)) to a more applicable form. The next chapter presents its solutions and their physical meaning.

3.3. Simplifying the master equation

In order to simplify the master equation given in Eq. (2.4), we must determine the components of the density matrix ρ on which the parity function depends. A perfect Hadamard gate transforms an arbitrary logical density matrix according to

$$\begin{bmatrix} 1-p & q \\ q^* & p \end{bmatrix}_L \longrightarrow \begin{bmatrix} \frac{1}{2}-\mathrm{Re}(q) & \frac{1}{2}-p+i\mathrm{Im}(q) \\ \frac{1}{2}-p-i\mathrm{Im}(q) & \frac{1}{2}+\mathrm{Re}(q) \end{bmatrix}_L , \tag{3.6}$$

where p and q are respectively the excited population $\langle 1|_L\, \rho\, |1\rangle_L$ and the coherence $\langle 1|_L\, \rho\, |0\rangle_L$. Note that logical 0 and 1 populations of the density matrix do not in general sum up to 1, but as explained in the next Section 3.4, this does not affect the sensing of the frequency ω. In this section, and for the remainder of this thesis, we will therefore assume that it is the case.

The parity function is equal to $\mathbb{P}_1 = \frac{1}{2} + \mathrm{Re}(q)$ which means that one has to solve the master equation solely for q. This problem reduces to finding the solution of a system of first-order differential equations,

$$\begin{cases} \dot{q} = (-3i\,\omega - 3\,\Gamma_{\mathrm{err}})\,q + (\Gamma_{\mathrm{err}} + \Gamma_{\mathrm{qec}})(e_1 + e_2 + e_3)\ , \\ \dot{e}_1 = \Gamma_{\mathrm{err}}\,q + (-i\omega - 3\,\Gamma_{\mathrm{err}} - \Gamma_{\mathrm{qec}})\,e_1 + \Gamma_{\mathrm{err}}\,(e_2^* + e_3^*)\ , \\ \dot{e}_2 = \Gamma_{\mathrm{err}}\,q + (-i\omega - 3\,\Gamma_{\mathrm{err}} - \Gamma_{\mathrm{qec}})\,e_2 + \Gamma_{\mathrm{err}}\,(e_1^* + e_3^*)\ , \\ \dot{e}_3 = \Gamma_{\mathrm{err}}\,q + (-i\omega - 3\,\Gamma_{\mathrm{err}} - \Gamma_{\mathrm{qec}})\,e_3 + \Gamma_{\mathrm{err}}\,(e_1^* + e_2^*)\ , \\ \dot{e}_1^* = \Gamma_{\mathrm{err}}\,q^* + (i\omega - 3\,\Gamma_{\mathrm{err}} - \Gamma_{\mathrm{qec}})\,e_1^* + \Gamma_{\mathrm{err}}\,(e_2 + e_3)\ , \\ \dot{e}_2^* = \Gamma_{\mathrm{err}}\,q^* + (i\omega - 3\,\Gamma_{\mathrm{err}} - \Gamma_{\mathrm{qec}})\,e_2^* + \Gamma_{\mathrm{err}}\,(e_1 + e_3)\ , \\ \dot{e}_3^* = \Gamma_{\mathrm{err}}\,q^* + (i\omega - 3\,\Gamma_{\mathrm{err}} - \Gamma_{\mathrm{qec}})\,e_3^* + \Gamma_{\mathrm{err}}\,(e_1 + e_2)\ , \\ \dot{q}^* = (3i\,\omega - 3\,\Gamma_{\mathrm{err}})\,q^* + (\Gamma_{\mathrm{err}} + \Gamma_{\mathrm{qec}})(e_1^* + e_2^* + e_3^*)\ . \end{cases} \tag{3.7}$$

It involves the matrix elements $q \coloneqq \langle 111|\,\rho\,|000\rangle$, $e_1 \coloneqq \langle 011|\,\rho\,|100\rangle$, $e_2 \coloneqq \langle 101|\,\rho\,|010\rangle$, $e_3 \coloneqq \langle 110|\,\rho\,|001\rangle$; and the dots denote their temporal derivatives. By noting that the system is invariant under permutation of erroneous components $\{e_1, e_2, e_3\}$, it can be further reduced to only four differential equations. In the matrix form these are

$$\frac{\mathrm{d}}{\mathrm{d}\tau}\begin{bmatrix} q \\ e \\ e^* \\ q^* \end{bmatrix} = \begin{bmatrix} -3i\omega - 3\Gamma_{\mathrm{err}} & \Gamma_{\mathrm{err}} + \Gamma_{\mathrm{qec}} & 0 & 0 \\ 3\Gamma_{\mathrm{err}} & -i\omega - 3\Gamma_{\mathrm{err}} - \Gamma_{\mathrm{qec}} & 2\Gamma_{\mathrm{err}} & 0 \\ 0 & 2\Gamma_{\mathrm{err}} & i\omega - 3\Gamma_{\mathrm{err}} - \Gamma_{\mathrm{qec}} & 3\Gamma_{\mathrm{err}} \\ 0 & 0 & \Gamma_{\mathrm{err}} + \Gamma_{\mathrm{qec}} & 3i\omega - 3\Gamma_{\mathrm{err}} \end{bmatrix} \begin{bmatrix} q \\ e \\ e^* \\ q^* \end{bmatrix}, \tag{3.8}$$

where $e \coloneqq e_1 + e_2 + e_3$ can be seen as a generalized error state. This reduced matrix differential equation is solved for uncorrected sensing in Section 4.1, and for the error-corrected situation in Section 4.2.

3.4. Offset of the parity function

In the previous section, we mentioned that the general formula for the parity signal is equal to $\frac{1}{2} + \mathrm{Re}(q(\tau))$. However, this is true if and only if populations to the logical states $|0\rangle_L$ and $|1\rangle_L$ sum to one. Unfortunately, this is not the case when the logical states are encoded in multiple qubits, since they also decay due to decoherence noise. Yet, as we show below this effect can be either corrected or, in some cases, even neglected.

In the situation where there is only one qubit in the system, both the logical and the full description of a density matrix coincide, such that the population in the excited state equals one minus the population in the ground state, i.e. $\langle 1|\,\rho\,|1\rangle = 1 - \langle 0|\,\rho\,|0\rangle$. However when one considers systems with more qubits, this statement no longer holds true since probabilities can be distributed across all the populations of ρ. Thus, after the free evolution, one should consider populations $p_0 = \langle 0|_L\,\rho\,|0\rangle_L$ and $p_1 = \langle 1|_L\,\rho\,|1\rangle_L$ as independent quantities. The second Hadamard gate (cf. Fig. 3.2A) transforms this density matrix

$$\begin{bmatrix} p_0 & \cdots & q \\ \vdots & \ddots & \\ q^* & & p_1 \end{bmatrix} \longrightarrow \begin{bmatrix} \frac{1}{2}(p_0 + p_1) - \mathrm{Re}(q) & \cdots & \frac{1}{2}(p_0 - p_1) + i\,\mathrm{Im}(q) \\ \vdots & \ddots & \\ \frac{1}{2}(p_0 - p_1) - i\,\mathrm{Im}(q) & & \frac{1}{2}(p_0 + p_1) + \mathrm{Re}(q) \end{bmatrix}. \tag{3.9}$$

Unlike Eq. (3.6), this transformation implies that the parity function is given by

$$\mathbb{P}_1(\tau) = \frac{1}{2}\big(p_0(\tau) + p_1(\tau)\big) + \mathrm{Re}(q(\tau)) \tag{3.10}$$

so that we have to determine not only the free evolution of the coherence q but also of p_0 and p_1. The dynamics of the latter are also dictated by the master equation (2.4). The particularity is, however, that it is not affected by the frequency ω, meaning that the first term in Eq. (3.10) can be seen as an offset, and the second as oscillations. The permutation invariant system of equations for p_0 and p_1 terms is given by Eq. (3.11) with $r_0 = \langle 100|\,\rho\,|100\rangle + \langle 010|\,\rho\,|010\rangle + \langle 001|\,\rho\,|001\rangle$ and similarly for r_1, but with two excited and one ground states. Hence, r_0 and r_1 represent the single error subspaces for populations p_0 and p_1 (similar to the e and e^* terms in Eq. (3.8)). The system of equations is then given by:

$$\frac{\mathrm{d}}{\mathrm{d}\tau}\begin{bmatrix}p_0\\r_0\\r_1\\p_1\end{bmatrix}=\begin{bmatrix}-3\Gamma_{\mathrm{err}} & \Gamma_{\mathrm{err}}+\Gamma_{\mathrm{qec}} & 0 & 0\\ 3\Gamma_{\mathrm{err}} & -3\Gamma_{\mathrm{err}}-\Gamma_{\mathrm{qec}} & 2\Gamma_{\mathrm{err}} & 0\\ 0 & 2\Gamma_{\mathrm{err}} & -3\Gamma_{\mathrm{err}}-\Gamma_{\mathrm{qec}} & 3\Gamma_{\mathrm{err}}\\ 0 & 0 & \Gamma_{\mathrm{err}}+\Gamma_{\mathrm{qec}} & -3\Gamma_{\mathrm{err}}\end{bmatrix}\begin{bmatrix}p_0\\r_0\\r_1\\p_1\end{bmatrix}. \tag{3.11}$$

Since the system is homogeneous, it is solvable based on the eigenanalysis of the matrix. The solution consists of a linear combination of products of each eigenvector with the exponential of the corresponding eigenvalue. The initial value of the problem is $(1/2, 0, 0, 1/2)$. The offset in the parity signal (3.10) is then:

$$\frac{1}{2}\big(p_0(\tau)+p_1(\tau)\big)=\frac{1}{2}\frac{\left(1+3\,\mathrm{e}^{-\tau(4\,\Gamma_{\mathrm{err}}+\Gamma_{\mathrm{qec}})}\right)\Gamma_{\mathrm{err}}+\Gamma_{\mathrm{qec}}}{4\,\Gamma_{\mathrm{err}}+\Gamma_{\mathrm{qec}}}\,. \tag{3.12}$$

Several points can be observed in this formula. First of all, in the case of no errors and no correction (i.e. $\Gamma_{\mathrm{err}}=\Gamma_{\mathrm{qec}}=0$), the offset is equal to $\frac{1}{2}$ which is exactly what we expect from an ideal Ramsey signal (cf. Eq. (3.3)). Secondly, this quantity decays over time such that it will reach a steady state, which in the case of no correction (i.e. $\Gamma_{\mathrm{qec}}=0$) will be $\frac{1}{8}$. The error rate Γ_{err} does not influence this value, it only controls how quickly this state is reached. Thirdly, one can also notice that for nontrivial Γ_{qec}, the offset reaches values closer to $\frac{1}{2}$ and with a perfect correction (i.e. $\Gamma_{\mathrm{qec}}\to\infty$) it will be exactly equal to the ideal line. Finally, the dynamics of q and $p_0/\,p_1$ have different time scales. Indeed, the oscillating part $\mathrm{Re}(q(\tau))$ is mainly dictated by the frequency ω,

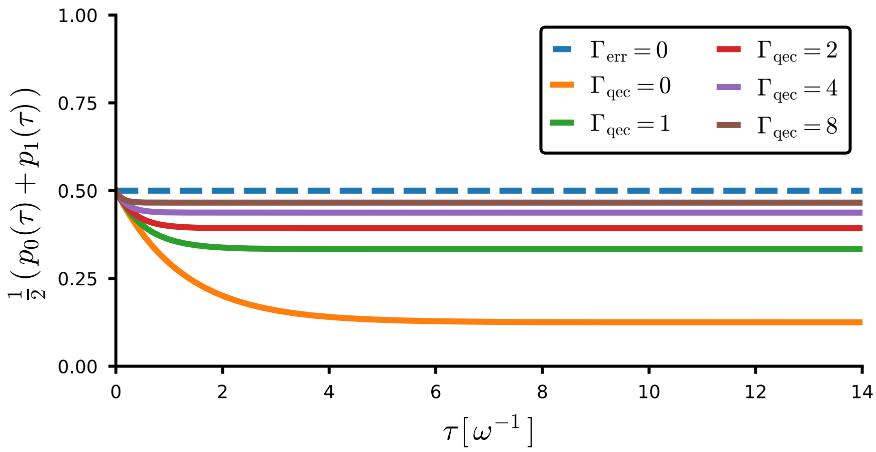

Figure 3.3.: *Dynamics of the parity function's offset.* It corresponds to half of the sum of the populations in $|0\rangle_L$ and $|1\rangle_L$ states. It dynamics is shown for several correction rates Γ_{qec} as well as for the ideal case (dashed), i.e. no errors and no correction.

whereas the offset is mostly determined by Γ_{qec}. Since we usually consider that $\Gamma_{\text{qec}} > \omega$, it follows that the populations p_0 and p_1 reach their steady state within one period of signal oscillation. This is the reason why in the scope of this work we assume the offset to be constant and equal to $\frac{1}{2}$. Moreover, this offset does not affect the sensing power of the Ramsey experiment, since a given time series can be first baseline corrected before being estimated with Eq. (3.1).

Fig. 3.3 shows the dynamics of the offset for different regimes. It is important to highlight that $\Gamma_{\text{qec}} \in \{1, 2, 4, 8\}[\omega]$ is a low correction rate. A more realistic and still low Γ_{qec} would be approximately 20ω, the offset using this value could then be considered ideal.

To conclude, Eq. (3.12) can also be used to study the asymptotic logical population as a function of error and correction rates. This is what is shown in Fig. 3.4 where the dashed line corresponds to the parameters for which this quantity is equal to 2/3. We can observe that the probability of finding our system in the logical subspace increases very quickly with Γ_{qec} which justifies our assumption from above.

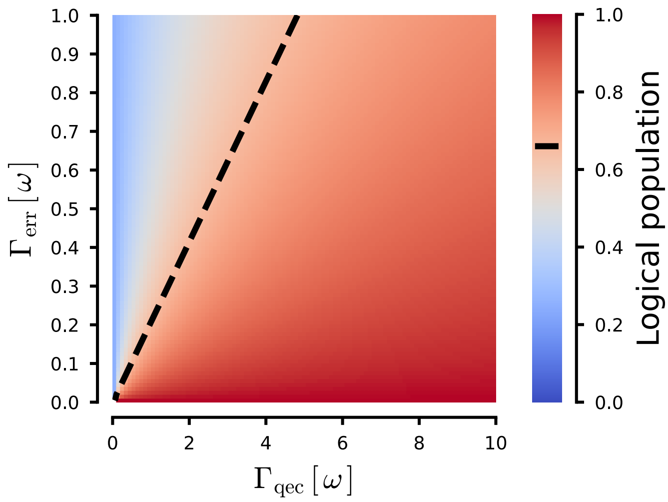

Figure 3.4.: *Asymptotic logical population.* Logical population $\lim_{\tau\to\infty} p_0(\tau) + p_1(\tau)$ derived from Eq. (3.12) plotted as a function of Γ_{err} and Γ_{qec}. The dashed line represents parameters for which this quantity is equal to 2/3.

CHAPTER 4

Solutions

In this chapter, we present the solutions of the permutation invariant problem given by Eq. (3.8) for various sensing situations. We then look at one intuitive physical interpretation of the parity functions that ensue from these solutions. At the end, we conclude with the validity of the simplified problem.

4.1. Uncorrected sensing

In a faulty but uncorrected Ramsey experiment, in other words for $\Gamma_{\mathrm{err}} > 0$ and $\Gamma_{\mathrm{qec}} = 0$, the system of equations presented in the previous chapter (cf. Eq. (3.8)) reads

$$\frac{\mathrm{d}}{\mathrm{d}\tau}\begin{bmatrix} q \\ e \\ e^* \\ q^* \end{bmatrix} = \begin{bmatrix} -3i\omega - 3\Gamma_{\mathrm{err}} & \Gamma_{\mathrm{err}} & 0 & 0 \\ 3\Gamma_{\mathrm{err}} & -i\omega - 3\Gamma_{\mathrm{err}} & 2\Gamma_{\mathrm{err}} & 0 \\ 0 & 2\Gamma_{\mathrm{err}} & i\omega - 3\Gamma_{\mathrm{err}} & 3\Gamma_{\mathrm{err}} \\ 0 & 0 & \Gamma_{\mathrm{err}} & 3i\omega - 3\Gamma_{\mathrm{err}} \end{bmatrix} \begin{bmatrix} q \\ e \\ e^* \\ q^* \end{bmatrix} . \tag{4.1}$$

This system can be, like for the populations p_0 and p_1 in Section 3.4, solved using the eigenanalysis of the matrix. The four eigenvalues of the matrix are

$$-3\Gamma_{\mathrm{err}} \pm 3\sqrt{\Gamma_{\mathrm{err}}^2 - \omega^2} \qquad\qquad -3\Gamma_{\mathrm{err}} \pm \sqrt{\Gamma_{\mathrm{err}}^2 - \omega^2} \ .$$

Based on the reasonable assumption that $\Gamma_{\mathrm{err}} < \omega$, the square roots can be rewritten such that the eigenvalues will have an imaginary part. The latter would be the cause of the oscillation of the Ramsey signal. The associated eigenvectors are not specified for the sake of simplicity. Solving the resulting linear system of equations with the initial value $(1/2, 0, 0, 1/2)$ and taking its real part leads to the following expression,

$$\begin{aligned} \mathrm{Re}(q(\tau)) = {} & \frac{1}{2}\frac{\omega^2}{D}\,\mathrm{e}^{-3\Gamma_{\mathrm{err}}\tau}\cos\!\left(3\sqrt{D}\,\tau\right) - \\ & - \frac{1}{2}\frac{\Gamma_{\mathrm{err}}^2}{(\sqrt{D})^3}\,\mathrm{e}^{-3\Gamma_{\mathrm{err}}\tau}\left(\sqrt{D}\cos^3(\sqrt{D}\,\tau) + \Gamma_{\mathrm{err}}\sin^3(\sqrt{D}\,\tau)\right) , \end{aligned} \tag{4.2}$$

where $D = \omega^2 - \Gamma_{\mathrm{err}}^2$. One can see that the first term follows from the first eigenvalue since it oscillates with $3\sqrt{D}$, while the second term contributes less to the signal because it scales as $\Gamma_{\mathrm{err}}^2\, D^{-1}$ whereas the first one as $\omega^2\, D^{-1}$.

Let us now assume that $\omega \gg \Gamma_{\text{err}}$, then the expansion of the scaling term gives:

$$\begin{aligned}\mathrm{Re}(q(\tau)) = &\frac{1}{2}\,\mathrm{e}^{-3\Gamma_{\text{err}}\tau}\,\cos\Big(3\sqrt{D}\,\tau\Big)\left[1+\left(\frac{\Gamma_{\text{err}}}{\omega}\right)^2+\mathcal{O}\left(\frac{\Gamma_{\text{err}}}{\omega}\right)^4\right]-\\ &-\frac{1}{2}\,\mathrm{e}^{-3\Gamma_{\text{err}}\tau}\,\cos^3(\sqrt{D}\,\tau)\left[\left(\frac{\Gamma_{\text{err}}}{\omega}\right)^2+\mathcal{O}\left(\frac{\Gamma_{\text{err}}}{\omega}\right)^4\right]-\\ &-\frac{1}{2}\,\mathrm{e}^{-3\Gamma_{\text{err}}\tau}\,\sin^3(\sqrt{D}\,\tau)\,\mathcal{O}\left(\frac{\Gamma_{\text{err}}}{\omega}\right)^4\end{aligned}$$

Following up on the previous observations about the importance of each element in Eq. (4.2), this expression shows that the second term starts to contribute only at second order in $\Gamma_{\text{err}}/\omega$. Moreover, it shows that the function $\mathrm{Re}(q(\tau))$ does not have a first-order approximation; in other words the 0-th order is true up to the second order.

$$\begin{aligned}&\text{0th order terms :} && \frac{1}{2}\,\mathrm{e}^{-3\Gamma_{\text{err}}\tau}\,\cos\Big(3\sqrt{D}\,\tau\Big)\\ &\text{2nd order terms :} && \frac{1}{2}\,\mathrm{e}^{-3\Gamma_{\text{err}}\tau}\left(\frac{\Gamma_{\text{err}}}{\omega}\right)^2\Big[\cos\Big(3\sqrt{D}\,\tau\Big)-\cos^3(\sqrt{D}\,\tau)\Big]\end{aligned}$$

In addition to this expansion, we expand the frequency of the trigonometric functions:

$$\sqrt{D} = \omega\left(1-\frac{1}{2}\frac{\Gamma_{\text{err}}^2}{\omega^2}+\mathcal{O}(\frac{\Gamma_{\text{err}}^4}{\omega^4})\right)$$

We finally can conclude that the parity function for an uncorrected sensing is given, up to second order in $\Gamma_{\text{err}}/\omega$, by

$$\mathbb{P}_1(\tau) = \frac{1}{2}+\frac{1}{2}\,\mathrm{e}^{-3\Gamma_{\text{err}}\tau}\,\cos[\,3\,\omega_{\text{eff}}\,\tau\,]\;, \tag{4.3}$$

where the effective frequency is $\omega_{\text{eff}} = \omega\left(1-\frac{1}{2}\frac{\Gamma_{\text{err}}^2}{\omega^2}\right)$. It is reasonable to consider such an expansion since it ensures a good enough contrast of the Ramsey signal, otherwise $\mathbb{P}_1(\tau)$ would be damped too quickly to observe any oscillations.

Interestingly, Eq. (4.3) highlights the presence of a bias that the well-established formula in Eq. (3.4) does not capture. Even though, in most cases, the scaling factor $1-\frac{1}{2}\frac{\Gamma_{\text{err}}^2}{\omega^2}$ in Eq. (4.3) is relatively low[i]. It can decrease to 0.94 in a worst case, where the error rate is three times lower than the frequency[ii]. For high precision sensing, it is thus important to take this bias into account.

[i] In preliminary observations (cf. Fig. 3.2), this factor is equal to 0.995 which is sufficiently small to be unnoticeable in the orange curve.

[ii] For $3\Gamma_{\text{err}} > \omega$, we assume that the contrast of Ramsey oscillation is too bad for sensing purposes.

4.2. Error-corrected sensing

In the situation where the correction rate Γ_{qec} is nontrivial, the matrix differential equation describing the evolution of the coherence q is given in Eq. (3.8) (also presented below). This permutation invariant system leads to a complicated set of rate equations which do not have, due to the presence of complex coefficients, a simple solution. A way to bypass this issue is to consider a slightly simpler problem given by the following matrix equation without the orange terms:

$$\frac{\mathrm{d}}{\mathrm{d}\tau}\begin{bmatrix} q \\ e \\ e^* \\ q^* \end{bmatrix} = \begin{bmatrix} -3i\omega - 3\Gamma_{\text{err}} & \Gamma_{\text{err}} + \Gamma_{\text{qec}} & 0 & 0 \\ 3\Gamma_{\text{err}} & -i\omega - 3\Gamma_{\text{err}} - \Gamma_{\text{qec}} & \mathbf{2\Gamma_{\text{err}}} & 0 \\ 0 & \mathbf{2\Gamma_{\text{err}}} & i\omega - 3\Gamma_{\text{err}} - \Gamma_{\text{qec}} & 3\Gamma_{\text{err}} \\ 0 & 0 & \Gamma_{\text{err}} + \Gamma_{\text{qec}} & 3i\omega - 3\Gamma_{\text{err}} \end{bmatrix}\begin{bmatrix} q \\ e \\ e^* \\ q^* \end{bmatrix}. \tag{4.4}$$

This approximation (i.e. removing the orange terms) can be understood as following: if a single-error state (e.g. $|010\rangle$ or $|001\rangle$) undergoes an additional bit flip on another qubit before being corrected, then the state is said to be lost, i.e. it ends up to be in a non-recoverable subspace of the Hilbert space. In reality, such a subspace does not exist and the system would remain in the single-error subspace but of opposite parity (using the previous example: the states become $|110\rangle$ and $|010\rangle$ if for instance $\sigma_x^{(1)}$ has occurred).

Mathematically, this means that the error components e and e^* of the density matrix ρ can only decay through bit flips into an additional virtual leakage subspace l. If one wants to monitor this variable, Eq. (4.4) has to be expanded by one equation to include l. We present this in Section 4.4. Conversely, replacing the $-3\Gamma_{\text{err}}\, e$ term by $-\Gamma_{\text{err}}\, e$ would lead to a closed system where double errors could not occur at all. The latter is a more restrictive assumption and was therefore not considered.

The problem together with the assumption explained above comes down to finding the eigenvalues and eigenvectors of the upper 2x2 matrix from Eq. (4.4). They are

$$\begin{aligned} \lambda_\pm &= -\frac{1}{2}\Gamma_{\text{qec}} - 3\,\Gamma_{\text{err}} - 2i\omega \pm \frac{1}{2}\sqrt{D} \\ \vec{v}_\pm \equiv \begin{bmatrix} v_\pm^q \\ v_\pm^e \end{bmatrix} &= \begin{bmatrix} \frac{1}{6\,\Gamma_{\text{err}}}\left(\Gamma_{\text{qec}} - 2i\,\omega \pm \sqrt{D}\right) \\ 1 \end{bmatrix}. \end{aligned} \tag{4.5}$$

where $D = \Gamma_{\text{qec}}^2 + 12\,\Gamma_{\text{qec}}\,\Gamma_{\text{err}} + 12\,\Gamma_{\text{err}}^2 - 4i\,\Gamma_{\text{qec}}\,\omega - 4\,\omega^2$ can be seen as a discriminant term. As mentioned in Section 3.4, the solution of the matrix differential equation is then given by the linear combination of the product of the eigenvectors with the exponentials of the respective eigenvalues,

$$\begin{bmatrix} q(\tau) \\ e(\tau) \end{bmatrix} = A\,\mathrm{e}^{\lambda_+\tau}\,\vec{v}_+ + B\,\mathrm{e}^{\lambda_-\tau}\,\vec{v}_-$$

where A and B have to be determined based on the initial values $q(0) = 1/2$ and $e(0) = 0$[iii]. It leads to the following expression for the coherence

$$q(\tau) = C_+ \,\mathrm{e}^{\frac{1}{2}\tau\left(-\Gamma_{\mathrm{qec}} - 6\Gamma_{\mathrm{err}} - 4i\omega + \sqrt{D}\right)} - C_- \,\mathrm{e}^{\frac{1}{2}\tau\left(-\Gamma_{\mathrm{qec}} - 6\Gamma_{\mathrm{err}} - 4i\omega - \sqrt{D}\right)} \,, \tag{4.6}$$

with the normalization constants

$$C_\pm = \frac{\Gamma_{\mathrm{qec}}}{4\sqrt{D}} - \frac{i\omega}{2\sqrt{D}} \pm \frac{1}{4} \,. \tag{4.7}$$

Finally, as mentioned in the previous chapter, the parity function corresponds to the real part of Eq. (4.6) offset by 1/2, thus:

$$\mathbb{P}_1(\tau) = \frac{1}{2} + \mathrm{Re}\left(C_+ \,\mathrm{e}^{\frac{1}{2}\tau\left(-\Gamma_{\mathrm{qec}} - 6\Gamma_{\mathrm{err}} - 4i\omega + \sqrt{D}\right)} - C_- \,\mathrm{e}^{\frac{1}{2}\tau\left(-\Gamma_{\mathrm{qec}} - 6\Gamma_{\mathrm{err}} - 4i\omega - \sqrt{D}\right)}\right) \,. \tag{4.8}$$

Due to a nontrivial $\sqrt{D}$ term[iv] in the exponential of the coherence $q(\tau)$, the parity function cannot take a simpler form than the latter one without being approximated.

4.3. Physical interpretation

In an error-corrected sensing situation, the solution presented above does not seem to have an intuitive physical explanation. Indeed, one can hardly distinguish a decaying part cause by errors from a growing part resulting from the error-correction. This is caused by the presence of the square-root term in the exponential. A way to circumvent this is to use an approximation to this term. Let us rewrite it as following:

$$\sqrt{D} = \Gamma_{\mathrm{qec}} \sqrt{1 + \frac{12\,\Gamma_{\mathrm{qec}}\,\Gamma_{\mathrm{err}} + 12\,\Gamma_{\mathrm{err}}^2 - 4i\,\Gamma_{\mathrm{qec}}\,\omega - 4\,\omega^2}{\Gamma_{\mathrm{qec}}^2}} \,. \tag{4.9}$$

Here, we have chosen to consider that the correction rate Γ_{qec} dominates over the rest of the terms in the square root. We expand it up to the second order of the fraction in the square root. The convergence of this expansion is ensured when the absolute value of this ratio is strictly lower than one; stated differently:

$$\begin{aligned} (12\,\Gamma_{\mathrm{qec}}\,\Gamma_{\mathrm{err}} + 12\,\Gamma_{\mathrm{err}}^2 - 4\,\omega^2)^2 + 16\,\Gamma_{\mathrm{qec}}^2\,\omega^2 - \Gamma_{\mathrm{qec}}^4 < 0 \\ (12\,\Gamma_{\mathrm{qec}}\,\Gamma_{\mathrm{err}} + 12\,\Gamma_{\mathrm{err}}^2 - 4\,\omega^2)^2 + 16\,\Gamma_{\mathrm{qec}}^2\,\omega^2 + \Gamma_{\mathrm{qec}}^4 > 0 \end{aligned} \tag{4.10}$$

have to be satisfied by the parameters of the system. While the bottom condition is always satisfied if $\Gamma_{\mathrm{err}} < \omega$, the top one has a nontrivial valid parameter space. Its validity limit is shown in Fig. 4.1 as a dashed line. Parameters inside the red region

[iii] As a remainder, we assumed that the logical Hadamard gates were ideal and transform therefore the initial $|0\rangle_L$ into the equal superposition $\frac{1}{\sqrt{2}}(|0\rangle_L + |1\rangle_L)$.

[iv] The discriminant is a complex number whose square root has no simple algebraic formula in terms of of ω, Γ_{err} and Γ_{qec}.

violate this condition meaning that the expansion does not converge. Assuming that we are in the green region, the coherence $q(\tau)$ given in Eq. (4.6) becomes:

$$q(\tau) \approx C_+ \underbrace{\exp\left[\tau\Big(-i(3\,\omega - 6\,\frac{\Gamma_{\text{err}}}{\Gamma_{\text{qec}}}\omega) - 6\,\frac{\Gamma_{\text{err}}}{\Gamma_{\text{qec}}}\,\Gamma_{\text{err}}\Big)\right]}_{\text{Evolution in the logical subspace}} -$$

$$- C_- \underbrace{\exp\left[\tau\Big(-i(\omega + 6\,\frac{\Gamma_{\text{err}}}{\Gamma_{\text{qec}}}\omega) - \Gamma_{\text{qec}} - 6\,\Gamma_{\text{err}} + 6\,\frac{\Gamma_{\text{err}}}{\Gamma_{\text{qec}}}\,\Gamma_{\text{err}}\Big)\right]}_{\text{Evolution in the erroneous subspace}} .$$

where we have considered only terms of the order $\mathcal{O}(1/\Gamma_{\text{qec}})$. In this assumption, the normalization constants become $C_+ = \frac{1}{2} - \frac{3}{2}\frac{\Gamma_{\text{err}}}{\Gamma_{\text{qec}}}$ and $C_- = -\frac{3}{2}\frac{\Gamma_{\text{err}}}{\Gamma_{\text{qec}}}$. Written in this way, one can identify two types of evolution:

The first one corresponding to the term C_+ is the evolution in the logical subspace which in the ideal case has a frequency of $3\,\omega$. Here, the frequency is biased such that its effective value (to first order in $\frac{\Gamma_{\text{err}}}{\Gamma_{\text{qec}}}$) is $\omega_{\text{eff}} = \omega(1 - 2\,\frac{\Gamma_{\text{err}}}{\Gamma_{\text{qec}}})$. In this situation, the scaling factor has a greater impact on the frequency than the one in the uncorrected case: if, as in Fig. 3.2, the correction rate is 50 times bigger than the error rate, then this factor equals 0.96. Moreover, in the uncorrected case oscillations decay at a rate $3\,\Gamma_{\text{err}}$, whereas in the presence of correction it decays at three times the effective error rate identified as

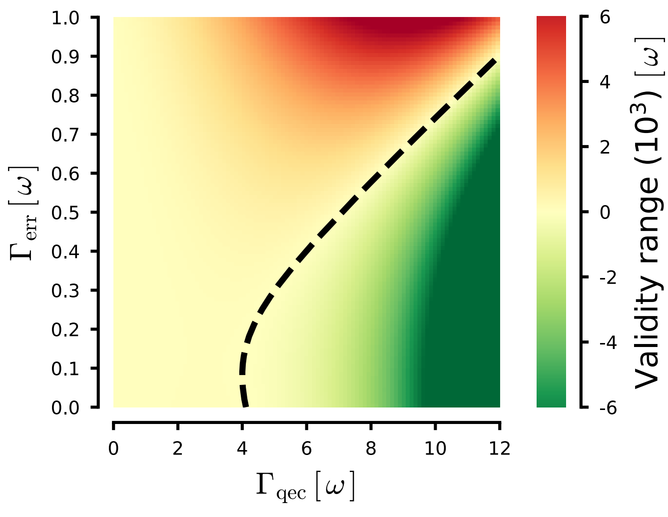

Figure 4.1.: *Validity range.* The validity condition (cf. top inequality of Eq. (4.10)) of the approximation given in Eq. (4.11) expressed in units of ω. The green region represents the valid parameter space and the red one – parameters which violate the condition. The dashed line is the limit between these areas.

$\Gamma_{\text{eff}} = 2\,\frac{\Gamma_{\text{err}}}{\Gamma_{\text{qec}}}\Gamma_{\text{err}}$.

The second evolution given by C_- denotes the evolution in the erroneous subspace which oscillates at a lower frequency. We observe that the correction considerably increases its frequency and decay rate. The latter as well as the small value of C_- will make this evolution quickly inconsiderable for the parity function.

All this allows us to reduce the previously stated parity function to only

$$\mathbb{P}_1(\tau) = \frac{1}{2} + \frac{1}{2}\,\mathrm{e}^{-3\,\Gamma_{\text{eff}}\,\tau}\cos[\,3\,\omega_{\text{eff}}\,\tau\,]\;, \tag{4.11}$$

where the effective parameters are

$$\begin{aligned} \omega_{\text{eff}} &= \omega\left(1 - 2\,\frac{\Gamma_{\text{err}}}{\Gamma_{\text{qec}}}\right)\;, \\ \Gamma_{\text{eff}} &= 2\,\frac{\Gamma_{\text{err}}}{\Gamma_{\text{qec}}}\Gamma_{\text{err}}\;. \end{aligned} \tag{4.12}$$

The measurement result in the presence of QEC can thus be cast into a form similar to the well-established equation (cf. Eq. (3.4)) but with a modified error rate and frequency. This shows us that the expected parity signal given in Eq. (3.5) is ultimately an incomplete and biased model of the situation.

At this point, a pertinent question is: how to explain such a bias in the parity signal? For answering this question, a discrete picture of the QEC process (cf. Fig. 2.1) can be helpful. As we mentioned above, the Hilbert space can be divided into logical and erroneous subspaces which evolve at different frequencies. The former is spanned by the logical states $|0\rangle_L$ and $|1\rangle_L$, whereas the latter by all the error states. A perfectly prepared equal superposition $|0\rangle_L + |1\rangle_L$ will evidently start in the logical subspace and will evolve at its frequency until a bit flip occurs. This error creates a channel connecting both subspaces. The state will then no longer evolve with $3\,\omega$ but only with ω until a second bit flip on the same qubit or until the next QEC operation. Since the correction rate Γ_{qec} is larger than the error rate Γ_{err}, the probability that the state is corrected through the QEC channel is higher. This implies that in the free evolution interval δt in-between two detection and correction operations, an extensive amount of it will be spent in the logical subspace, and the remainder in the erroneous subspace. Finally, the total phase the state has accumulated at the end of the waiting time simply corresponds to the time spent in each subspace multiplied the respective frequency. The disparity in the frequencies is thus the origin of the bias.

The scheme presented in Fig. 4.2 summarizes the physical interpretation described above. The chronometers portray the time spent in the subspaces and the speedometers their frequency. The size of the bubbles emphasizes the probability of finding the system in the corresponding subspace, while the arrows depict the channels connecting these two regions.

In the uncorrected sensing, the bias results from the same effect as in the corrected case, namely the dissimilarity in the evolution in each subspace. However, here the

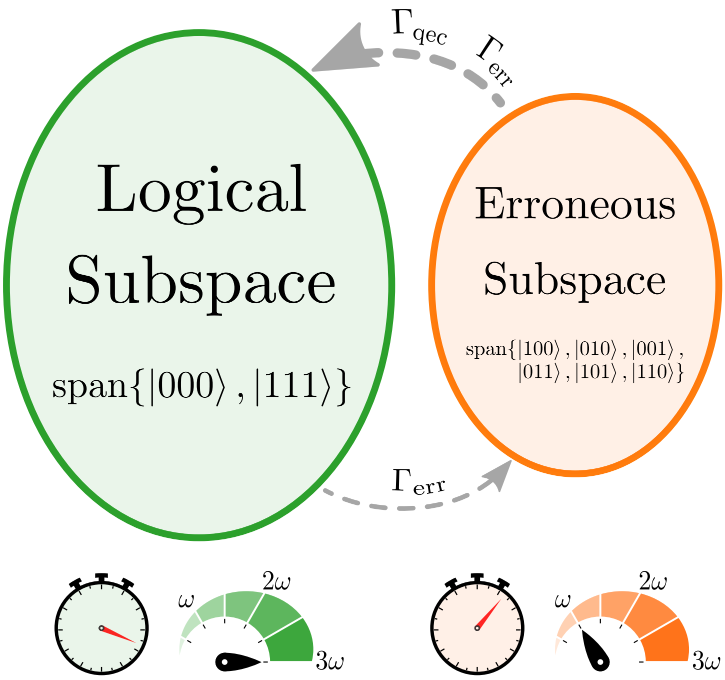

Figure 4.2.: *Physical interpretation of the logical and erroneous subspaces.* The chronometers portray the time spent by the system in the subspaces and the speedometers – the frequencies of the evolution in the corresponding region. The disparity between the evolution-frequencies in the logical and erroneous subspaces is the reason for the bias, since the total phase acquired by the state is the time spent in each subspace times the respective frequency.

situation would be symmetrical (i.e. bubbles of same size), since only the error channels allow the transfer of the state from one subspace to the other.

4.4. Validity of the simplified problem

As mentioned in Section 4.2, the proposed solution (cf. Eq. (4.8)) has been derived from a much simpler problem than the original one. The simplified matrix differential equation was constructed such that it ensures the existence of a subspace from which the coherence q cannot be recovered. We refer to the population of this subspace as l. The initial system of ODEs (cf. Eq. (3.7)) would then acquire an additional equation describing the dynamics of this population. After applying the permutation invariance as well as the assumption from Section 4.2, we end up with the matrix equation:

$$\frac{\mathrm{d}}{\mathrm{d}\tau}\begin{bmatrix} q \\ e \\ l \\ e^* \\ q^* \end{bmatrix} = \begin{bmatrix} -3i\omega - 3\Gamma_{\rm err} & \Gamma_{\rm err}+\Gamma_{\rm qec} & 0 & 0 & 0 \\ 3\Gamma_{\rm err} & -i\omega - 3\Gamma_{\rm err} - \Gamma_{\rm qec} & 0 & 0 & 0 \\ 0 & 2\Gamma_{\rm err} & 0 & 2\Gamma_{\rm err} & 0 \\ 0 & 0 & 0 & i\omega - 3\Gamma_{\rm err} - \Gamma_{\rm qec} & 3\Gamma_{\rm err} \\ 0 & 0 & 0 & \Gamma_{\rm err}+\Gamma_{\rm qec} & 3i\omega - 3\Gamma_{\rm err} \end{bmatrix}\begin{bmatrix} q \\ e \\ l \\ e^* \\ q^* \end{bmatrix}, \tag{4.13}$$

It has mostly the same form as Eq. (4.4) but with coupling terms in orange now populating the leakage subspace l. Moreover, it can still be seamlessly solved using the eigenanalysis of the matrix, because l does not participate in any way in the dynamics of q or e. In other words, l decouples the upper two equations (q, e) from the bottom two (q^*, e^*).

The matrix in Eq. (4.13) has five eigenvalues: a trivial one $\lambda_0 = 0$, two eigenvalues $\lambda_{1,2} = \lambda_\pm$, and the last two, $\lambda_{3,4} = \lambda_\pm^*$ with $\lambda_\pm$ as defined in Eq. (4.5). The last two eigenvalues are the eigenvalues of the lower 2x2 block of the matrix. The solution of the differential equation with initial parameters $(q, e, l) = (1/2, 0, 0)$ is then identical to Eq. (4.6) for the coherence q. The solution for the error component e reads

$$e(\tau) = \frac{3\,\Gamma_{\rm err}}{2\sqrt{D}}\,\mathrm{e}^{\frac{1}{2}\tau\left(-\Gamma_{\rm qec}-6\Gamma_{\rm err}-4i\omega+\sqrt{D}\right)} - \frac{3\,\Gamma_{\rm err}}{2\sqrt{D}}\,\mathrm{e}^{\frac{1}{2}\tau\left(-\Gamma_{\rm qec}-6\Gamma_{\rm err}-4i\omega-\sqrt{D}\right)} \tag{4.14}$$

and is very similar to evolution of the coherence component (cf. Eq. (4.6)).

An interesting quantity to look at is the leakage subspace population and its dynamics. As for q and e, it has some time-dependent terms which will lead to decaying oscillations when we consider their real part. However, it also has a constant term which means that after a long enough time τ:

$$l(\tau) \xrightarrow[\tau\to\infty]{} \frac{4\,\Gamma_{\rm err}^4 - 2\,\omega^2\,\Gamma_{\rm err}^2}{\omega^4 + 12\,\omega^2\,\Gamma_{\rm err}^2 + 8\,\omega^2\,\Gamma_{\rm err}\,\Gamma_{\rm qec} + 4\,\Gamma_{\rm err}^4 + \omega^2\,\Gamma_{\rm qec}^2}\ .$$

This is an unnatural behavior since in a real situation this subspace would not exist but would instead be expressed as fluctuations between e and e^*. This constant typically needs to be much lower than the population of the other subspaces taken individually during the sensing time. To ensure the validity of the reduced problem one can take an even stronger constraint, namely $|l(\tau = \infty)| \ll 1$, which means solving the inequality:

$$\frac{4\,\Gamma_{\rm err}^4 - 2\,\omega^2\,\Gamma_{\rm err}^2}{12\,\omega^2\,\Gamma_{\rm err}^2 + 4\,\Gamma_{\rm err}^4 + 8\,\omega^2\,\Gamma_{\rm err}\,\Gamma_{\rm qec} + \omega^2\,\Gamma_{\rm qec}^2 + \omega^4} \ll 1\ .$$

This leads to the condition:

$$\Gamma_{\rm qec} \gg -4\Gamma_{\rm err} \pm \sqrt{2\Gamma_{\rm err}^2 - \omega^2} \qquad \text{along with} \qquad \Gamma_{\rm err}\,(\omega^2 - 2\Gamma_{\rm err}^2) \neq 0\ .$$

Knowing that we typically have $\Gamma_{\rm err} \ll \omega$ and $\Gamma_{\rm qec} \in \mathbb{R}$, we can claim that this stronger constraint is usually satisfied.

The dynamics of $|q(\tau)|$, $|e(\tau)|$, $|l(\tau)|$ for a very low correction rate are shown in Fig. 4.3. This plot also shows the simulations of $|q(\tau)|$ and $|e(\tau)|$. They agree well with the analytically derived functions except for small oscillations which come from the coupling of the two pairs of equations (q, e) and (q^*, e^*) in Eq. (3.7). These fluctuations disappear for larger correction rates.

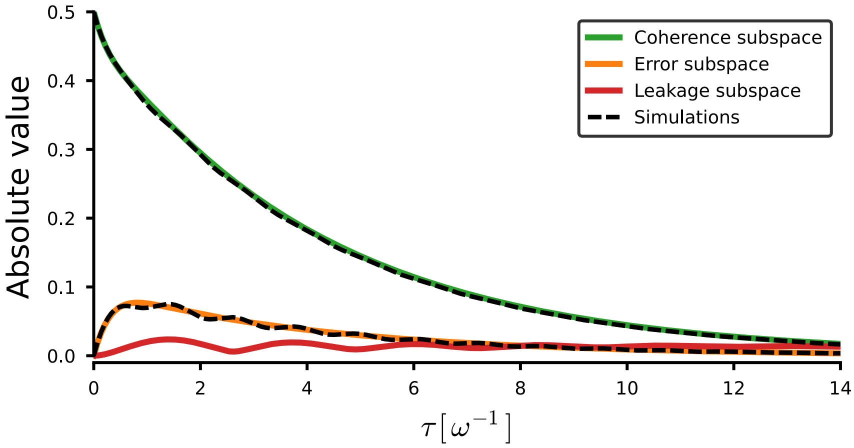

Figure 4.3.: *Dynamics of the subspaces.* Dynamics of the populations of the coherence (q), the single-error (e) and the leakage (l) subspaces as dictated by the matrix differential equation (4.13). A very low correction rate was chosen to emphasize oscillations in the simulations which, for higher correction rates, get damped.

Chapter 5

Solution analysis

In this chapter, we analyse the solutions of the estimation problem mentioned in Section 3.1. In particular, we argue in the first section that, due to the form of the solutions derived in the previous chapter, there is a need to switch from a univariate estimation problem given by Eq. (3.1), to a multivariate one, i.e. where the estimator is no more a scalar but a vector. Then, using a biased estimator theory, we show that the canonical form of the parity function (cf. Eq. (3.4)) leads to a biased estimator. Moreover, impacts of the proposed solution (cf. Eq. (4.8)) on the protocol's sensitivity and on the Fourier transform of $\mathbb{P}_1$ are also discussed. Finally, in the last section, we propose an adaptive sensing protocol which optimizes the number of measurements needed for the estimation problem.

5.1. Principal component analysis

The estimation problem as stated in Eq. (3.1) is univariate, which means that the error and correction rates on which $\hat{\omega}$ depends remain constant throughout the minimization process. This raises a fundamental question: How do we compare estimators which result from different parity functions $\mathbb{P}_1$? Indeed, if the expected parity function, given in Eq. (3.5), reflects the true outcome of any Ramsey experiment, it would mean that the decay rate Γ_{eff} is always decoupled from the frequency ω. In other words, fixing the former to a certain value would not affect much the estimation power of the other. On the contrary, if the proposed solution (cf. Eq. (4.8)) is a closer representation of the true parity function, then Γ_{eff} and ω_{eff} are both dependent on each other (as showed in Eq. (4.12)) which means that fixing one of them could be detrimental for the estimation of the other.

A multivariate estimation problem would then be a solution to these concerns, because a two-dimensional minimization problem is able to, using appropriate algorithms, capture the variability of parameters which are estimated. The problem reads

$$\begin{bmatrix} \hat{\theta}_1 \\ \hat{\theta}_2 \end{bmatrix} = \underset{\{\theta_1, \theta_2\}}{\arg\min} \sum_{\tau} \Big[X_\tau - \mathbb{P}_1(\tau, \theta_1, \theta_2, \Gamma_{\text{qec}}) \Big]^2 , \tag{5.1}$$

where now the estimator is a two-dimensional vector. An important aspect to highlight is that, with this expression, we assume the correction rate Γ_{qec} to be a known and fixed parameter. This is a reasonable assumption, because as mentioned in Chapter 2.1 it can in principle be engineered and thus set by the experimenter before proceeding with the sensing protocol. Moreover, the multivariate estimation solves the issue of determining the value of the decay rate which could be experimentally arduous.

Both the well-established and the proposed parity functions can be summarized by a unique expression,

$$\mathbb{P}_1(\tau,\theta_1,\theta_2,\Gamma_{\rm qec}) = \tfrac{1}{2} + \tfrac{1}{2}\,\mathrm{e}^{-3\,f_\Gamma(\theta_1,\theta_2,\Gamma_{\rm qec})\,\tau}\cos[3\,f_\omega(\theta_1,\theta_2,\Gamma_{\rm qec})\,\tau]$$

$$f_\Gamma(\theta_1,\theta_2,\Gamma_{\rm qec}) = \theta_1$$

$$f_\omega(\theta_1,\theta_2,\Gamma_{\rm qec}) = \theta_2$$

$$f_\Gamma(\theta_1,\theta_2,\Gamma_{\rm qec}) = 2\,\frac{\theta_1}{\Gamma_{\rm qec}}\theta_1$$

$$f_\omega(\theta_1,\theta_2,\Gamma_{\rm qec}) = \theta_2\,(1-2\,\frac{\theta_1}{\Gamma_{\rm qec}})$$

The decay rate together with the frequency are now functions of these new variables $\hat{\theta}_1$ and $\hat{\theta}_2$. The definition of these functions is given in the left box (dark red) for the standard $\mathbb{P}_1$ (cf. Eq. (3.4)) and in the right one (dark green) for the proposed parity (cf. Eq. (4.8)). We preserve this color code for the rest of the chapter. We can now proceed with testing the estimation power of these functions.

First, we conduct a principal component analysis (PCA). This is a widely used technique in data analysis which aims to "reduce the dimensionality of a dataset, while preserving as much 'variability' (i.e. statistical information) as possible" [42]. Here we use this technique for determining the directions that maximize the variance of our estimator. We start by simulating a set of data points using a Monte Carlo simulation of

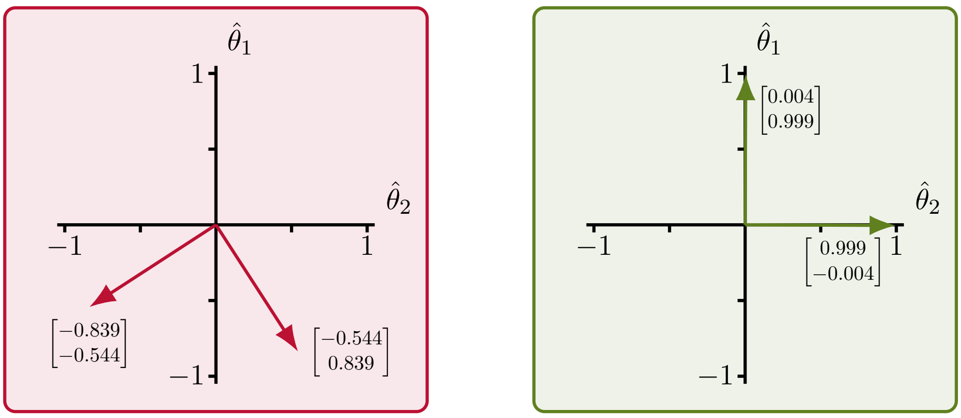

Figure 5.1.: *Principal components analysis.* Arrows points toward the directions that maximize the variance of the estimator given in Eq. (5.1). The left (dark red) box shows the result for the estimator resulting from the well-established parity function and the right (dark green) box – for the proposed function.

the problem. Then, using the non-linear least square solver from the Python NumPy library [43], we obtain an estimate of the vector $[\hat{\theta}_1\,,\,\hat{\theta}_2]^\intercal$, as well as its covariance matrix. The trends of the variance, the so-called principal components, are given by the eigenvectors of this matrix. Fig. 5.1 represents these directions for both estimators. We see that the principal components of the canonical estimator do not lay on the axis of $\hat{\theta}_1$ and $\hat{\theta}_2$, meaning that the obtained estimates are linearly correlated. Conversely, this is not the case for the proposed estimator; here the two directions coincide with the system of coordinates.

It is important to keep in mind that this analysis only considers the result of one estimation process. For another set of data points, the covariance matrices will be different and thus the position of the arrows might change. However, after performing the PCA on multiple data sets with various values of simulation parameters (ω, Γ_{err}, Γ_{qec}), no divergences from this conclusion have been observed. From now on, we will refer to $[\hat{\theta}_1\,,\,\hat{\theta}_2]^\intercal$ as to $[\hat{\Gamma}_{\mathrm{err}}\,,\,\hat{\omega}]^\intercal$ to avoid confusion when speaking of parity function's parameters.

5.2. Numerical comparison

A first measure of the estimators' performance is the absolute error between a reference signal and its closest fit. Fig. 5.2A shows this quantity for both estimators as a function of the sensing time τ. The reference signal was produced by a master equation solver from the QuTiP [41] library. The figure highlights that the estimator resulting from the proposed solution consistently outperforms the canonical one by at least one order of magnitude.

The same performance comparison is also shown in Fig. 5.2B where the reference data points were no longer calculated via QuTiP but taken from Reiter, Sørensen, Zoller, and Muschik [25], Fig. 6. In this paper, the authors presented a continuous and dissipative QEC scheme for

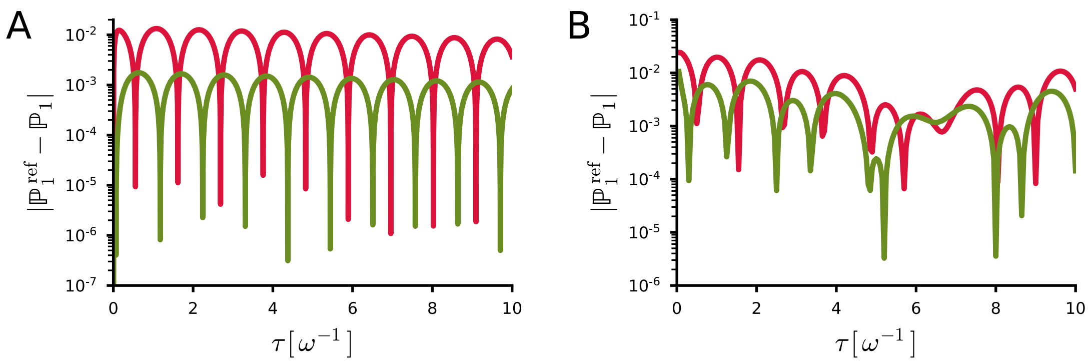

Figure 5.2.: *Absolute error* between a reference Ramsey signal and the fitted functions. The fitted function were the canonical equation (3.4) (dark red) and the proposed solution (4.8) (dark green). Reference data were: **A.** numerically calculated using QuTiP; **B.** obtained from Reiter, Sørensen, Zoller, and Muschik [25].

a trapped ion quantum system. Their simulation is arguably more sophisticated than our previous one, since it takes into account various couplings and auxillary modes. These data can thus be seen as a robustness test for both estimators. Despite a higher absolute error than in Fig. 5.2A, the proposed estimator still produces a closer fit to the reference data.

Another important performance metric is the root-mean-square error (RMSE) is defined as

$$\mathrm{RMSE}(\mathbb{P}_1^{\mathrm{ref}}, \mathbb{P}_1) = \sqrt{\frac{1}{N} \sum_{\tau}^{N-1} \left| \mathbb{P}_1^{\mathrm{ref}}(\tau) - \mathbb{P}_1(\tau) \right|^2} \, . \tag{5.2}$$

Here N – the total number of time step, measures the expected value of the square error between the reference signal $\mathbb{P}_1^{\mathrm{ref}}$ and an arbitrary function $\mathbb{P}_1$ over the time τ. For instance, the RMSE for the red and green fits from Fig. 5.2B are respectively 0.8% and 0.3% confirming the conclusions we draw above. This metric can also help to verify that the proposed Ramsey signal follows, in different regimes, an expected behavior: that is for perfect QEC, it should equal the ideal signal and for weak QEC, the signal should tend toward the uncorrected parity function derived in Eq. (4.3). The former can be straightforwardly concluded from the reduced solution (cf. Eq. (4.11)), since, in the limit $\Gamma_{\mathrm{qec}} \to \infty$, effective parameters defined in Eq. (4.12) tend to $\Gamma_{\mathrm{eff}} \to 0$ and $\omega_{\mathrm{eff}} \to \omega$.

The regime of an uncorrected Ramsey signal is characterized by a correction rate which is significantly lower than the error rate, $\Gamma_{\mathrm{qec}} \ll \Gamma_{\mathrm{err}}$. In this situation, the parity function resulting from the coherence $q(\tau)$ given in Eq. (4.6) takes the following form

$$\mathbb{P}_1(\tau) = \frac{1}{2} + \frac{1}{2} \mathrm{e}^{-3\Gamma_{\mathrm{err}}\tau} \cos\left[3\,\omega_{\mathrm{eff}}\,\tau\right] + \mathcal{O}\left(\mathrm{e}^{-\Gamma_{\mathrm{err}}\tau} \left(\frac{\Gamma_{\mathrm{err}}}{\omega} \right)^2 \right) \tag{5.3}$$

when expanding it under the assumption of $\Gamma_{\mathrm{qec}} \to 0$ and $\Gamma_{\mathrm{err}} \ll \omega$. As mentioned in Section 4.1, the reason for the expansion in orders of $\Gamma_{\mathrm{err}}/\omega$ is that this ratio is directly related to the contrast of the Ramsey signal. Once this gets close to 1, the oscillations are damped more quickly. Here the effective frequency is equal to

$$\omega_{\mathrm{eff}} = \frac{\omega}{3} \left(2 + \sqrt{1 - 3\left(\frac{\Gamma_{\mathrm{err}}}{\omega} \right)^2} \right) = \omega \left(1 - \frac{1}{2} \left(\frac{\Gamma_{\mathrm{err}}}{\omega} \right)^2 + \mathcal{O}\left(\frac{\Gamma_{\mathrm{err}}^4}{\omega^4} \right) \right) .$$

This expansion is exactly the same as the one derived for the uncorrected sensing, meaning that up to the second order in $\Gamma_{\mathrm{err}}/\omega$ both Eq. (5.3) and Eq. (4.3) are equal.

Fig. 5.3 shows the RMSE between an ideal Ramsey signal (reference) and the proposed parity function for different Γ_{qec}. For weak correction, the RMSE is constant due to the fact that the parity is mainly equal to the constant function $\mathbb{P}_1 = 0.5$. However, when the correction becomes strong enough the error converges also toward a constant value due to rounding errors.

Finally, the ultimate performance comparison is the absolute error between the reference parameters and the estimates $\hat{\Gamma}_{\mathrm{err}}$ and $\hat{\omega}$ because these are the quantities we

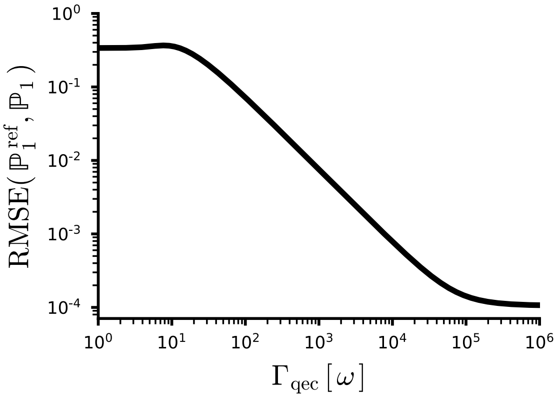

Figure 5.3: *Regime of perfect QEC.* Root-mean-squared error (RMSE), as defined in Eq. (5.2), between an ideal Ramsey signal (cf. Eq. (3.3)) and the proposed parity function (cf. Eq. (4.8)) for different correction strengths. As Γ_{qec} approaches the perfect QEC, the discrepancy reaches the level of rounding errors.

seek, especially the frequency which contains the information about the signal to sense. Fig. 5.4 illustrates how this error for $\hat{\omega}$ looks like for a fixed error and an increasing correction rates. We can observe that here again the proposed estimator beats the standard one by at least one order of magnitude. The figure also contains the same analysis for a three-parameter estimator which was realized with the modified parity function but with no prior knowledge about the correction rate. Overall, it shows a worse performance than in the two-parameter case, i.e. the green line is most of the time below the dashed one. Nonetheless, it is always better or equal to the two-parameter estimator built upon the canonical formula. Its performance could eventually be improved by tuning hyper-parameters of the minimization algorithm.

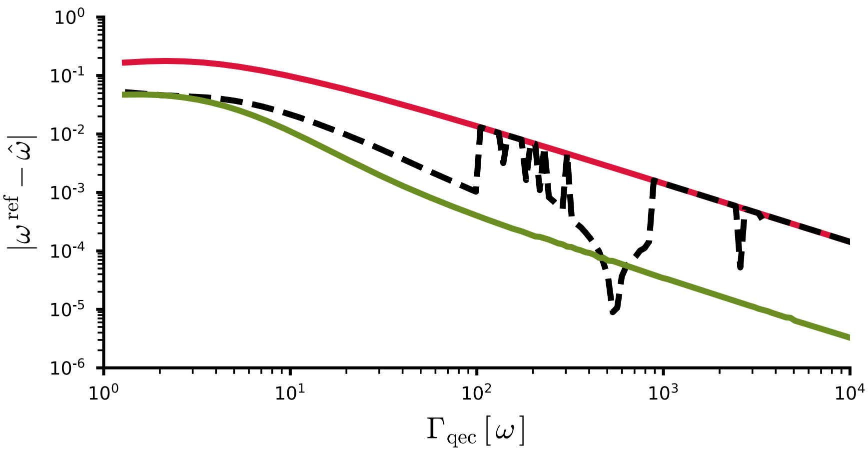

Figure 5.4.: *Absolute error of frequency estimate.* Absolute error between the frequency of the reference parity signal and its estimate $\hat{\omega}$. Full lines represent two-parameter estimators built upon the standard equation (3.4) (dark red) and the proposed solution (4.11) (dark green). The dashed line shows a three parameters estimator using also the proposed function but with the third parameter being Γ_{qec}.

5.3. Biased estimator theory

In this section, we aim to show that the estimator derived from Eq. (4.8) is unbiased, whereas the established parity function Eq. (3.4) gives a biased estimator of the true frequency ω. In statistics and more precisely in the estimation theory, any unbiased estimator has to satisfy the so-called Cramèr-Rao lower bound (CRB) [44] which limits the variance of the estimator to be at least as large as the inverse of the Fisher information (FI). For the univariate case stated in Eq. (3.1), the theorem reads

$$\mathrm{Var}(\hat{\omega}) \geq (\, n\,\mathcal{I}(\omega)\,)^{-1} \; . \tag{5.4}$$

In this expression, n denotes the total number of observations. The FI can be seen as the total information accessible by the system and thus depends only on the true frequency ω. These two quantities are defined by

$$\mathrm{Var}(\hat{\omega}) = \mathbb{E}[(\hat{\omega} - \mathbb{E}[\hat{\omega}])^2] \qquad \text{and} \qquad \mathcal{I}(\omega) = \mathbb{E}\left[\left(\frac{\partial}{\partial\omega}\log\mathbb{P}(X|\omega)\right)^2\right] \; . \tag{5.5}$$

Some optimized and finer bounds have been previously derived [5], based on the use of the quantum Fisher information. Nevertheless, as our measurement scheme is chosen and fixed, such technicalities are not necessary and the lower bound given by Eq. (5.4) is adequate.

The inequality in Eq. (5.4) can be exploited to establish whether an estimator is biased. Practically, if for a given probability density function $\mathbb{P}(X|\omega)$, one observes that the variance is lower than the CRB, one can claim that $\hat{\omega}$ is biased. We will refer to this specific case as the violation of the CRB. Conversely, if the bound is satisfied, no further conclusion can be drawn. Stated differently, this is a sufficient but not necessary condition.

However, as argued previously, we must consider a two-parameter least-squares regression such that the estimation problem is not univariate anymore. Nevertheless, the CRB can be naturally extended [45] to the unbiased multivariate case. It takes the form of a matrix condition where the variance and the Fisher information are replaced by their matrix counterparts, respectively the covariance $\mathbf{Cov}(\hat{\Theta})$ and the Fisher information $\mathbf{I}(\Theta)$ matrices,

$$\mathbf{Cov}(\hat{\Theta}) - \frac{1}{n}\,\mathbf{I}(\Theta)^{-1} \geq 0 \tag{5.6}$$

where $\hat{\Theta} = [\,\hat{\theta}_1\,,\,\hat{\theta}_2\,]^{\mathrm{T}}$ is an unbiased estimator. This condition is often difficult to verify, but due to the fact that both matrices are positive semi-definite, the following corollary is directly derived from Eq. (5.6) [46],

$$\mathrm{Tr}\Big(\mathbf{Cov}(\hat{\Theta})\Big) \;=\; \mathrm{Var}(\hat{\theta}_1) + \mathrm{Var}(\hat{\theta}_2) \;\geq\; \frac{1}{n}\,\mathrm{Tr}\Big(\mathbf{I}(\Theta)^{-1}\Big) \;\geq\; \frac{1}{n}\big(\mathcal{I}(\hat{\theta}_1)^{-1} + \mathcal{I}(\hat{\theta}_2)^{-1}\big) \; . \tag{5.7}$$

Here the left-hand side can be seen as the total variance of the estimator. In this expression, $\mathrm{Tr}(\,\cdot\,)$ denotes the trace of a matrix. We now derive an expression for the FI knowing that the random variable X can take only two values, $x \in \{0\,,\,1\}$:

$$\begin{aligned}
\mathcal{I}(\theta) &= \sum_{x=0}^{1} \mathbb{P}(X=x|\theta)\left[\frac{\partial}{\partial\theta}\log\mathbb{P}(X=x|\theta)\right]^2 = \\
&= \mathbb{P}(X=1|\theta)\left[\frac{\partial}{\partial\theta}\log\mathbb{P}(X=1|\theta)\right]^2 + \mathbb{P}(X=0|\theta)\left[\frac{\partial}{\partial\theta}\log\mathbb{P}(X=0|\theta)\right]^2 = \\
&= \frac{1}{\mathbb{P}(X=1|\theta)}\left[\frac{\partial}{\partial\theta}\mathbb{P}(X=1|\theta)\right]^2 + \frac{1}{1-\mathbb{P}(X=1|\theta)}\left[\frac{\partial}{\partial\theta}\mathbb{P}(X=1|\theta)\right]^2 = \\
&= \frac{1}{\mathbb{P}(X=1|\theta)(1-\mathbb{P}(X=1|\theta))}\left[\frac{\partial}{\partial\theta}\mathbb{P}(X=1|\theta)\right]^2
\end{aligned}$$

In our case, the estimator is defined as $\hat{\Theta} = [\,\hat{\Gamma}_{\text{err}}\,,\,\hat{\omega}\,]^{\intercal}$ and the conditional probabilities $\mathbb{P}(X|\theta)$ correspond to the parity function $\mathbb{P}_1(\tau)$ with all the parameters fixed, except θ. To be explicit, we can express elements on the right-hand side of inequality (5.7) as

$$\mathcal{I}(\theta)^{-1} = \mathbb{P}_1(\tau)\,(1-\mathbb{P}_1(\tau))\left[\frac{\partial\mathbb{P}_1(\tau)}{\partial\theta}\right]^{-2}\;, \tag{5.8}$$

with $\theta \in \{\,\Gamma_{\text{err}}, \omega\,\}$. For the frequency, this formula is known as the sensitivity (squared).

As mentioned above, the violation of the CRB is a sufficient condition for an estimator to be biased, that is, if one monitors a transgression of inequality (5.7), one can infer that $\hat{\omega}$ does not equal the true value. A Monte-Carlo simulation is appropriate for this because it allows to choose the number of observations n, in contrast to a master equation simulation. This is what was used in Fig. 5.5A. It shows the total variance for estimators obtained with the parity functions Eq. (3.4) (diamonds) and Eq. (4.6) (circles) as well as the right-hand side of Eq. (5.7) (dashed). Each point on this plot embodies one regression for a total of 1500. One observes that the estimator obtained from the standard parity function consistently violates the CRB. Hence, we come to the conclusion that it is biased. The modified estimator using the proposed parity function also transgresses the lower bound for $\tau \gtrapprox 250$, but this happens when the system's parity is around 0.5, i.e. when the quantum information is fully corrupted.

Fig. 5.5B shows the value of the frequency bias which was obtained using

$$\text{Bias}(\hat{\omega}) = \mathbb{E}[(\omega-\hat{\omega})^2] - \text{Var}(\hat{\omega})\;. \tag{5.9}$$

The former term characterize the mean square deviation of the estimate $\hat{\omega}$ from its true value ω. From Fig. 5.5, we can see that the proposed solution has a lower bias but a greater total variance compared to the well-established parity function. This reflects the so-called bias-variance tradeoff [47]. It is, however, important to highlight that the main contribution to the total variance comes from $\text{Var}(\hat{\Gamma}_{\text{err}})$ and that $\text{Var}(\hat{\omega})$ is minimal for the proposed parity function. Lastly, the flatness of the bias for the well-established function comes from the simplicity of the model which makes it converge to a stable and constant local minimum.

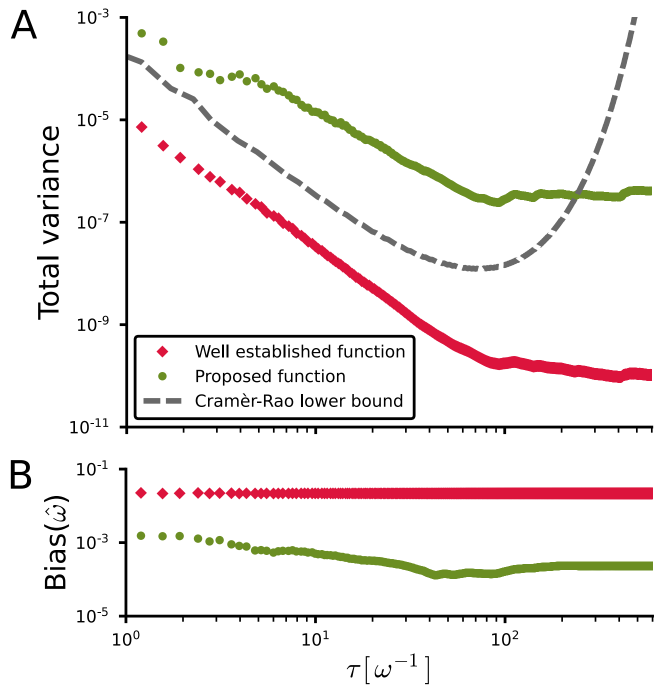

Figure 5.5: **A.** Total variance as a function of the sensing time τ for estimators ensued from Eq. (3.4) (diamonds) and Eq. (4.8) (circles). The plot also shows the right-hand side of the Cramèr-Rao lower bound as stated in Eq. (5.7). The well-established formula consistently violates this inequality. **B.** Bias (cf. Eq. (5.9)) of the frequency estimate $\hat{\omega}$ as a function of τ. Each point was obtained from a multivariate least-squares regression of data simulated with the Monte-Carlo method.

5.4. Sensitivity

The sensitivity is a key quantity in any sensing experiment. It is defined as the minimum detectable signal per unit time. In a Ramsey protocol it translates into the minimum detectable variation of the frequency ω, often labelled $|\delta\omega|(\tau)$. The lower bound of the sensitivity is called the Standard Quantum Limit (SQL) and is obtained by inserting the ideal parity function into Eq. (5.8) and taking its square root. In our case, the SQL takes the form

$$|\delta\omega|(\tau) = (9\,n\,\tau^2)^{-1/2}\,, \tag{5.10}$$

which in a logarithmic coordinate system is a decreasing line. Stated differently, in an decoherence-free situation, the precision of the frequency estimate improves for long waiting times τ.

In the presence of errors, this no longer holds true. For the standard parity function given by Eq. (3.4), the sensitivity is equal to [40]

$$|\delta\omega|_{\mathrm{std}}(\tau) = \sqrt{\frac{1 - \mathrm{e}^{-6\,\Gamma_{\mathrm{err}}\,\tau}\,\cos^2[\,3\,\omega\,\tau\,]}{n\,9\,\tau^2\,\mathrm{e}^{-6\,\Gamma_{\mathrm{err}}\,\tau}\,\sin^2[\,3\,\omega\,\tau\,]}} \tag{5.11}$$

for which the minimum is attained at the optimal sensing time

$$\tau_{\mathrm{opt}} = \frac{\pi}{2}\frac{k_{\mathrm{opt}}}{3\,\omega} \quad \text{with} \quad k_{\mathrm{opt}} = \left\lfloor \frac{2}{\pi}\frac{\omega}{\Gamma_{\mathrm{err}}} \right\rceil \tag{5.12}$$

where k_{opt} is the optimal integer and $\lfloor \cdot \rceil$ indicates the rounding to the nearest integer. Roughly speaking, τ_{opt} can be inferred with $(3\,\Gamma_{\text{err}})^{-1}$.

The sensitivity for the proposed parity function (4.8) can also be derived from Eq. (5.5) (for $\theta \equiv \omega$). For this, we must derive an analytical formula for the differential of $\mathbb{P}_1(\tau)$ with respect to ω:

$$\frac{\partial \mathbb{P}_1}{\partial \omega} = \text{Re}\left(-2i\tau\, q(\tau) + \Delta q(\tau)\right) \;, \tag{5.13}$$

with

$$\begin{aligned}
\Delta q(\tau) &= \Delta C_+\, \mathrm{e}^{\frac{1}{2}\tau\left(-\Gamma_{\text{qec}}-6\Gamma_{\text{err}}-4i\omega+\sqrt{D}\right)} - \Delta C_-\, \mathrm{e}^{\frac{1}{2}\tau\left(-\Gamma_{\text{qec}}-6\Gamma_{\text{err}}-4i\omega-\sqrt{D}\right)} \\
\Delta C_\pm &= \frac{1}{4(D)^{3/2}}\left[-2i(D-\Gamma_{\text{qec}}^2) - \tau\sqrt{D}(i\Gamma_{\text{qec}}+2\omega)(\pm\Gamma_{\text{qec}} \mp 2i\omega + \sqrt{D})\right] \;.
\end{aligned}$$

Due to the complexity of this formula, we obtain at the end a much more elaborate sensitivity than the one presented in Eq. (5.11). To be explicit, the full expression of the sensitivity for an error-corrected Ramsey experiment is given by the following equation

$$|\delta\omega|_{\text{mod}}(\tau) = \sqrt{\frac{1}{n}\mathbb{P}_1(\tau)\left(1-\mathbb{P}_1(\tau)\right)}\left[\frac{\partial \mathbb{P}_1(\tau)}{\partial \omega}\right]^{-1} \;, \tag{5.14}$$

where $\mathbb{P}_1(\tau)$ has to be substituted with the proposed parity function in Eq. (4.8) and the partial derivative with Eq. (5.13).

As an alternative, we can also derive the sensitivity using the reduced form of $\mathbb{P}_1$ which is presented in Eq. (4.11). Due to the requirement of performing a partial derivative with respect to ω, we must opt for higher order approximations of the effective decay rate and frequency[i]. That is to say that Γ_{eff} and ω_{eff} have to be considered as functions of ω. Thus, the sensitivity is given by

$$|\delta\omega|_{\text{mod}}(\tau) = \sqrt{\frac{1-\mathrm{e}^{-6\,\Gamma_{\text{eff}}\,\tau}\,\cos^2[\,3\,\omega_{\text{eff}}\,\tau\,]}{n\,9\,\tau^2\,\mathrm{e}^{-6\,\Gamma_{\text{eff}}\,\tau}\left((\partial_\omega\Gamma_{\text{eff}})\,\cos[\,3\,\omega_{\text{eff}}\,\tau\,] + (\partial_\omega\omega_{\text{eff}})\,\sin[\,3\,\omega_{\text{eff}}\,\tau\,]\right)^2}} \;. \tag{5.15}$$

Fig. 5.6 shows how this equation deviates from the full expression presented above. We can see that the first-order approximations in $1/\Gamma_{\text{qec}}$ of the effective parameters give a very loose approximation of the expected curve[ii]. The precision, however, converges to 1 when we increase the approximation order.

An important aspect to mention is that this formula has almost the same form as the standard sensitivity derived in Eq. (5.11), except that now we have $\partial_\omega\omega_{\text{eff}}$ and $\partial_\omega\Gamma_{\text{eff}}$ terms in the denominator. A numerical study of the ratio of this terms [i] shows that in the validity range (cf. Fig. 4.1) the former extensively dominates over the second one.

[i] See details in Appendix B

[ii] Even though all the parameters satisfy the validity conditions settled by inequalities (4.10).

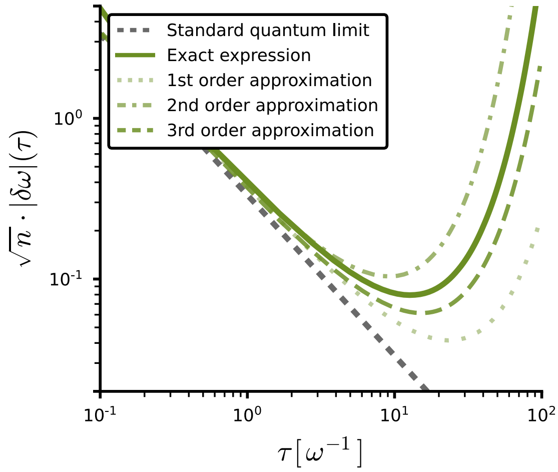

Figure 5.6: *Error-corrected Ramsey experiment's sensitivity.* The exact curve was obtained by plugging the proposed parity function (4.8) into Eq. (5.8) and taking its square root. The other curves where obtained in the same way but with different orders of approximation of the proposed parity function where the first order corresponds to the reduced equation (4.11).

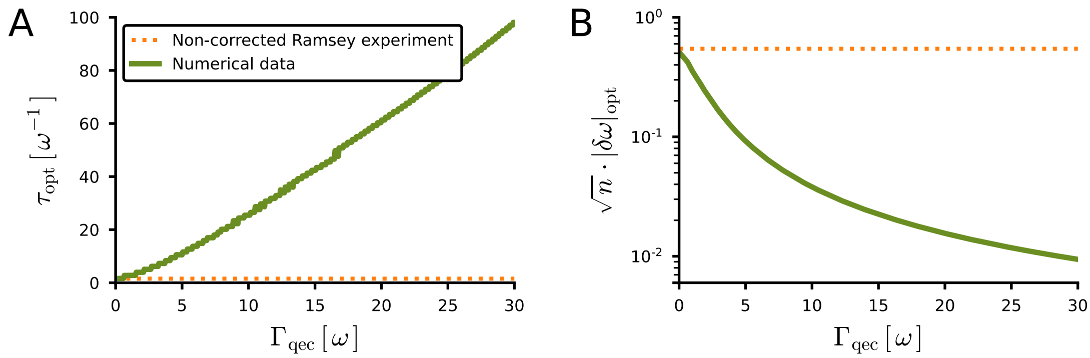

Figure 5.7.: *Optimal sensing time and sensitivity.* Plots of the optimal sensing time τ_{opt} (A) and sensitivity $|\delta\omega|_{\text{opt}}$ (B) as functions of the correction rate Γ_{qec}. These data were obtained numerically based on Eq. (5.14).

We then conclude the relationship

$$|\delta\omega|_{\text{std}}(\tau) \approx |\partial_\omega \omega_{\text{eff}}|\; |\delta\omega|_{\text{mod}}(\tau) = \left|1 - 2\,\frac{\Gamma_{\text{err}}}{\Gamma_{\text{qec}}}\right|\; |\delta\omega|_{\text{mod}}(\tau)\ . \tag{5.16}$$

This relation highlights the fact that depending on the model we chose for describing the system, the sensitivity of the protocol is potentially overestimated, i.e. better (lower) than the true one, since the partial derivative of ω_{eff} with respect to the frequency is less than one.

Moreover, this description indicates that we can calculate the optimal sensing time in a similar manner as in Eq. (5.12).

$$\tau_{\text{opt}} = \frac{\pi}{2}\frac{k_{\text{opt}}}{3\,\omega_{\text{eff}}} \qquad \text{with} \qquad k_{\text{opt}} = \left\lfloor \frac{2}{\pi}\frac{\omega_{\text{eff}}}{\Gamma_{\text{eff}}} \right\rceil \tag{5.17}$$

but, as mentioned previously, it can as well be roughly inferred with $(3\,\Gamma_{\text{eff}})^{-1}$. Fig. 5.7 illustrates how τ_{opt} and the optimal sensitivity $|\delta\omega|_{\text{opt}} \equiv |\delta\omega|(\tau_{\text{opt}})$ evolve with the correction rate. Unsurprisingly, both quantities get enhanced when Γ_{qec} increases. It is, however, worth noting that $|\delta\omega|_{\text{opt}}$ exhibits a steeper improvement for low corrections than for high ones, which demonstrates that QEC has a non-negligible impact on the sensitivity of the protocol even if it induces a systematic bias.

A reasonable question to ask now is: how do can we determine if the sensitivity is under- or overestimated? A method to verify this is to directly compare the theoretical curves $|\delta\omega|_{\text{std}}(\tau)$ and $|\delta\omega|_{\text{mod}}(\tau)$ to the sensitivity calculated with raw data. However, the latter can be sometimes difficult to evaluate since it requires the reconstruction of the Ramsey signal and thus a large number of measurement rounds. We propose here an alternative method:

Consider a set of observations for which a frequency $\hat{\omega}$ and an error rate $\hat{\Gamma}_{\text{err}}$ were estimated using the well-established parity function Eq. (3.4). Then, in the biased scenario $\hat{\omega} \equiv \omega$ and $\hat{\Gamma}_{\text{err}} \equiv \Gamma_{\text{err}}$, we can directly insert them in Eq. (5.11) and calculate a first curve. If instead we assume the existence of a bias, then the estimated parameters stand for ω_{eff} and Γ_{eff}, respectively, which substituted into Eq. (5.14) give a second curve. These two functions are presented in Fig. 5.8 as dashed and dotted lines, respectively. Although both of them satisfy the standard quantum limit, only one reflects the true sensitivity of the system. The tool which helps to discriminate it is the optimal sensing time τ_{opt}. Indeed, in both situations, the estimated $\hat{\tau}_{\text{opt}}$ depends only on $\hat{\Gamma}_{\text{err}}$ and is calculated by $(3\,\hat{\Gamma}_{\text{err}})^{-1}$. As we can see in Fig. 5.8, $\hat{\tau}_{\text{opt}}$ coincides with the minimum of only one of the two curves. Thus, one can conclude that, in this instance, the second model is the more faithful approximation to the true sensitivity.

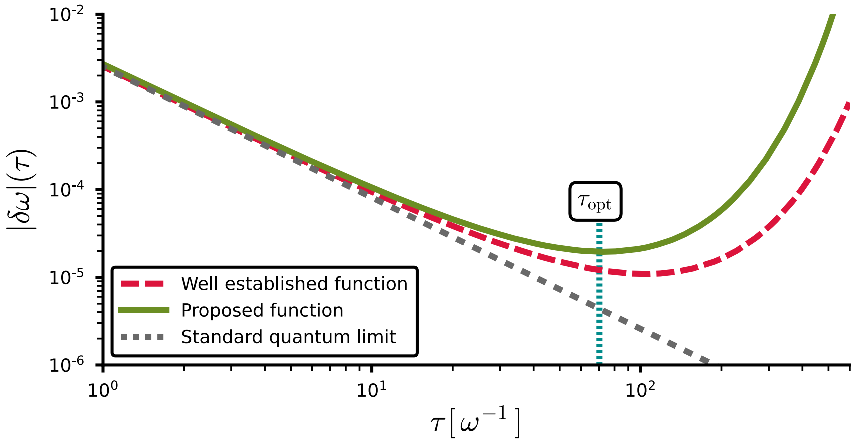

Figure 5.8.: *Sensitivities comparison.* Two different models are compared: biased sensitivity (dashed) and modified one (solid) obtained with Eq. (5.11) and (5.14),respectively. Both functions were plotted for the same values of ω and Γ. The optimal sensing time τ_{opt}, estimated from $(3\,\hat{\Gamma}_{\text{err}})^{-1}$, helps to discriminate which model reflects the true sensitivity of the system.

5.5. Fourier transform of a Ramsey signal

Since the goal of Ramsey interferometry is to sense the frequency of the measured signal, discrete Fourier transform (DFT) seems to be an appropriate technique for this as displayed in Fig. 3.2C.

Let us use this technique to highlight how the bias evolves for an increasing correction rate. This evolution is shown in Fig. 5.9. While the reduced parity function given in Eq. (4.11) can help to approximate this curve for large Γ_{qec}, for low values, the validity conditions (cf. Eq. (4.10)) are not satisfied anymore. We can observe that after reaching a minimum, the effective frequency starts to increase again. This is an expected phenomena since, in the limit $\Gamma_{\text{qec}} \to 0$, the bias should tend toward the expression from the uncorrected solution presented in Eq. (4.3). A justified question to ask is: why does the bias increase, in the first place, for low correction rates?

This arises from the nature of the measurement we are using. Indeed, when the measurement basis is made of logical states, qubits from the erroneous subspace do not corrupt the outcome, such that the only way they bias the measurement is due to multiple bit flips. However, the probability of these events is low, since, as shown in Fig. 3.3, the qubits population, initially in the logical states, will quickly and equally spread among all the possible states of the Hilbert space. When QEC becomes significant, this probability starts to increase together with the logical population (cf. Fig. 3.4). A non-negligible fraction of the latter has, however, spent some time in the erroneous subspace and thus evolved at a different frequency (as explained in Section 4.3). As we keep increasing Γ_{qec}, this time decreases, which consequently reduces the bias.

We now analyse the Fourier transform (FT) of various solutions to the Ramsey sequences. For an ideal parity signal (cf. Eq. (3.3)), it will simply correspond to a delta function which peaks at $3\,\omega$. The FT of the proposed solution is however much more arduous. To find it, we can consider the reduced solution given in Eq. (4.11). Then, our goal is to calculate the FT of the function: $f(\tau) = \mathrm{e}^{-3\,\Gamma_{\text{eff}}\,\tau}\cos(3\,\omega_{\text{eff}}\,\tau)$ The resulting

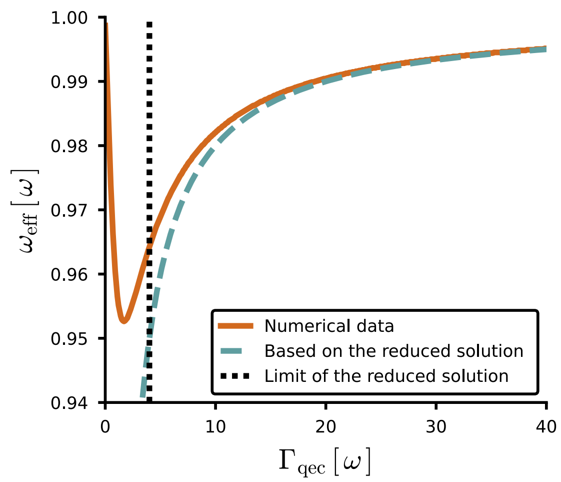

Figure 5.9: *Bias vs QEC.* Evolution of the effective frequency in terms of correction rate. Numerical data were obtained using a discrete Fourier transform of the proposed solution (cf. Eq. (4.8)). The curve is well approximated by the first order expression of ω_{eff} derived in Eq. (4.12). The limit of this approximation is set by inequalities (4.10).

FT then reads[iii]:

$$\tilde{f}(\underline{\omega}) = \frac{1}{2\sqrt{2\pi}} \left(\frac{1}{3\,\Gamma_{\mathrm{err}} + i(\underline{\omega} - 3\,\omega_{\mathrm{eff}})} + \frac{1}{3\,\Gamma_{\mathrm{err}} + i(\underline{\omega} + 3\,\omega_{\mathrm{eff}})} \right) .$$

In practice one usually considers the magnitude of a FT to determine the main frequencies of the original signal. In our case that means:

$$|\tilde{f}(\tau)| = \frac{1}{2\sqrt{2\pi}} \frac{4\,\underline{\omega}^2 + 36\,\Gamma_{\mathrm{eff}}^2}{\underline{\omega}^4 - 18(\omega_{\mathrm{eff}}^2 - \Gamma_{\mathrm{eff}}^2)\underline{\omega} + 81(\omega_{\mathrm{eff}}^2 + \Gamma_{\mathrm{eff}}^2)^2} \tag{5.18}$$

Notice that the numerator of this rational function is a constantly increasing function for $\underline{\omega} > 0$ and that the denominator has no real roots[iv]. $|\tilde{f}|$ will then peak at $\underline{\omega}$ where the denominator is at its minimum, because away from this point it will quickly dominate over the numerator. The derivative of the denominator has three real roots but only $\underline{\omega}_{\mathrm{max}} = 3\sqrt{\omega_{\mathrm{eff}}^2 - \Gamma_{\mathrm{eff}}^2}$ is pertinent in the given situation, since it is the only strictly positive one. We can see that it conforms to what we expect, namely that it peaks at $\underline{\omega} \approx 3\,\omega_{\mathrm{eff}}$ in the validity range of the reduced parity function.

5.6. Adaptive sensing protocol

The sensing protocol that we have presented in Section 3.1 is the most basic usable protocol, when dealing with a Ramsey interferometry experiment. However, one requires a lot of experimental data before starting to look at the estimation problem itself. Indeed, each point from the set $\{X_\tau\}$ is one occurrence of the random variable X for a given sensing time. This means that for being relatively confident about its value, we must repeat the experiment with the same interval τ several times and then average the resulting values. The issue with this procedure is that the amount of information we accumulate, while repeating the experiments, is used only once, at the end. Here we propose how it can be optimized by efficiently extracting information about the system at each run of the protocol.

Let us first look at the discrete QEC as stated in Section 2.2. In this situation, after each measurement round, we have access to several quantities: First, we can roughly estimate the correction rate Γ_{qec}. If the gates are applied periodically as shown in Fig. 2.1, we divide the number of QEC gates $n_{\mathcal{R}}$ by the sensing time τ that, at the end, would simply correspond to $(\delta t)^{-1}$. If otherwise the gates are distributed randomly in time, the estimate is obtained through a weighted arithmetic mean where each correction process is weighted by the time interval since a previous $\mathcal{R}$ gate.

[iii] The result does not exactly correspond to the Fourier transform of $f(\tau)$, but to $f(\tau)\,\Pi(\tau)$ where $\Pi(\tau)$ is known as window or pulse function. In our case, we have chosen a rectangular function which is equal to identity in the interval $(0, \tau)$ and zero otherwise. Moreover, in Fig. 3.2C, the time series were restricted exclusively to this interval which explains why we do not see a sinc behavior expected for the Fourier transforms.

[iv] The discriminant is negative and equal to $-(6\,\omega_{\mathrm{eff}}\,\Gamma_{\mathrm{eff}})^4$.

Secondly, we have access to all the syndromes which come along with QEC. These quantities, produced during the error detection, are key elements that allow us to determine which qubit in the code word is erroneous and thus condition its correction. For a three qubit repetition code, each syndrome is a two-bit string established by the eigenvalues of $\sigma_z^{(1)}\sigma_z^{(2)}$ and $\sigma_z^{(2)}\sigma_z^{(3)}$. If, for instance, the syndrome is 01, we conclude that there is an error in the third qubit and, similarly, if it is equal to 11, then the second one is erroneous. Knowing all the syndromes in one run of the protocol, we can assess, to a certain extent, the error rate Γ_{err} by dividing the number of erroneous syndromes $n_{\mathcal{E}}$ (i.e. different from 00) by the sensing time τ. Here, as for the estimation of Γ_{qec}, we can also implement a weighted average with weights exponentially depending on the time interval between $\mathcal{R}$ gates[v].

Having an estimate of these two rates makes it possible to evaluate the amount of bias the Ramsey signal has. Indeed, the expression of the effective frequency ω_{eff} given in Eq. (4.12)[vi] lets us estimate this value without the need of knowing the true frequency.

Finally, in a similar way, we can approximate the effective decay rate Γ_{eff}. This in turn helps to compute the optimal sensing time as $\tau_{\mathrm{opt}} \sim (3\,\Gamma_{\mathrm{eff}})^{-1}$. This time is afterwards used to adapt the protocol toward the optimal sensitivity point $|\delta\omega|_{\mathrm{opt}}$.

The algorithm presented with these four points will, at first, result in a very sparse series of Ramsey experiments with various free evolution times but, as the protocol keeps repeating, all the parameters presented above will eventually converge to their definite value. Such convergence is due to the fact that before estimating $\omega_{\mathrm{eff}}/\omega$, Γ_{eff} and τ_{opt}, we are also averaging Γ_{qec} and Γ_{err} with all their estimates from previous runs. Fig. 5.10 depicts the whole sensing protocol where the adaptive steps explained above are indicated as a calibration phase. Indeed, we can see it as such, because it allows us to infer some parameters of the system but not to estimate the true frequency ω. For the latter, several methods exist:

As already explained one may fit the proposed solution to several oscillations measured by tweaking the sensing time around its optimal value τ_{opt}. Alternatively, a quantum phase estimation algorithm can as well be implemented [7]. However, the quantum sensing community is often interested in the detection of small signals, which in this case, are considered as perturbations $\delta V(t)$ of a known background $V_0(t)$. The two main methods commonly utilized are the slope and the variance detection. The quantity, that we are then interested in, is $\delta\mathbb{P}(\tau) = \mathbb{P}(\tau) - \mathbb{P}_1(\tau_0)$ with a suitably chosen τ_0. For the slope detection, we pick this initial point such that it maximizes the slope of the parity function, whereas for the variance detection, we select its crest (i.e. minimal slope). These points lie around the optimal sensing duration τ_{opt}[vii] due to its property of minimizing the sensitivity $|\delta\omega|$. This justifies once again the name “Calibration” for the adaptive algorithm presented above.

[v] The longer is the time interval, the higher is the probability that a quantum jump occurs.
[vi] For a better approximation, see Appendix B.
[vii] For the slope detection, this point is actually $\tau_0 = \tau_{\mathrm{opt}}$.

This scheme, explained using a discrete implementation of QEC, can also be used in a dissipative case with specific techniques of monitoring the environmental degrees of freedom. In a trapped ion implementation, a solution would be to monitor photon recoils as suggested by Plenio and Huelga [23].

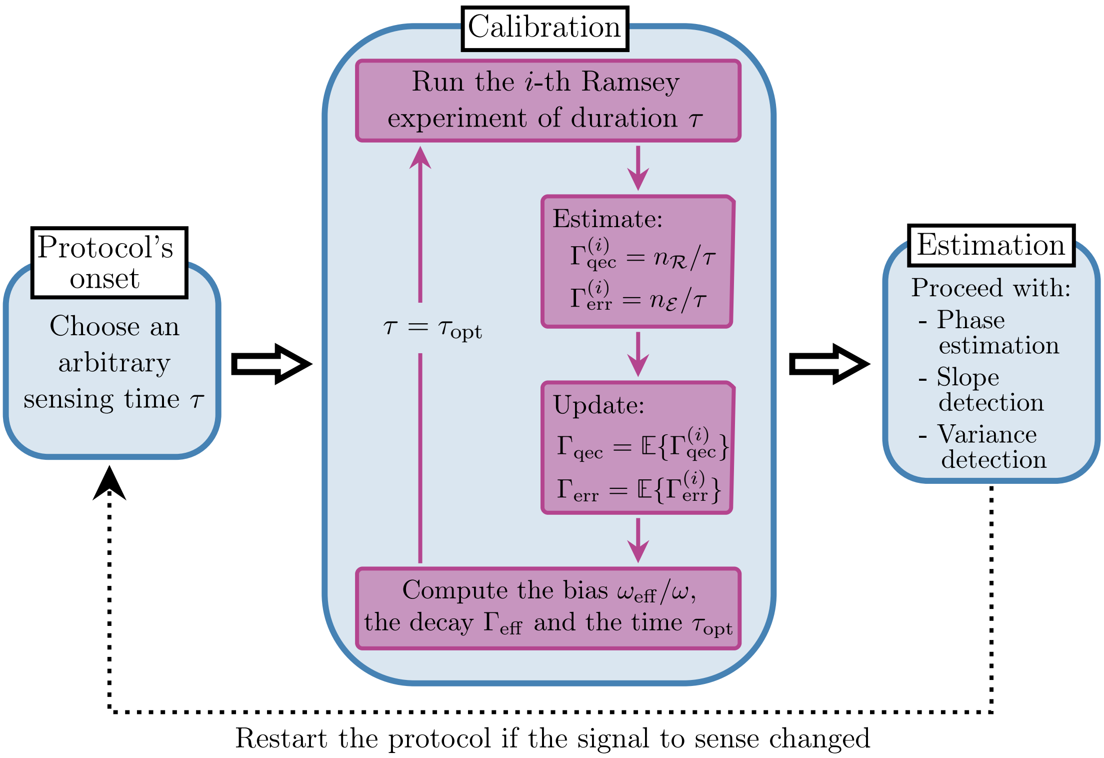

Figure 5.10.: *Adaptive sensing protocol.* The adaptive part is implemented in the *Calibration* phase where the length of the Ramsey experiment is tuned depending on the quantities Γ_{qec} and Γ_{err} estimated from previous measurement rounds. $n_{\mathcal{R}}$ and $n_{\mathcal{E}}$ are respectively the number of QEC gates and the number of detected errors during one run. Unlike in this scheme, one can as well implement a weighted arithmetic mean for the estimators. The *Update* step is a simple averaging over the previous runs' values.

Chapter 6

Generalization

All the results presented so far concerned specifically the three-qubit repetition code. It can, though, be consistently extended to other codewords as long as the evolution frequencies in the logical and erroneous subspaces differ. In this chapter, we present how the size of the repetition code (i.e. the number of two-level systems) influences the parity signal and the proposed solution.

6.1. Larger repetition codes

Let us start to look at encodings involving more than three qubits, i.e. $\{|0\rangle_L, |1\rangle_L\} \equiv \{|0\rangle^{\otimes N}, |1\rangle^{\otimes N}\}$. The signal hamiltonian $H(t)$ and the error jump operators $L_{\text{err}}^{(j)}$ are defined in the same way as the three qubit case and the QEC jump operators (for correcting single errors) can also be easily extended as following,

$$L_{\text{qec}}^{(j)} = \sqrt{\Gamma_{\text{qec}}}\, \sigma_x^{(j)} \prod_{k\neq j}^{N-1} \frac{1 - \sigma_z^{(j)}\, \sigma_z^{(k)}}{2} \, . \tag{6.1}$$

Although the system of equations obtained from the master equation (2.4) would grow exponentially with N, it can be lowered by assuming their permutation invariance as in (3.8). That said, the system will not be simplified to only four equations, since we have to consider the presence of higher-order error subspaces. Indeed, in the three-qubit case, the double-error subspace, with respect to $|1\rangle_L$, was spanned by $\{|100\rangle, |010\rangle, |001\rangle\}$, which means that it overlapped with the single-error space of the logical 0 state. Mathematically speaking, this overlap was translated as a coupling of e and e^* in Eq. (3.8).

If instead we assume four-qubit code words, there exists a distinct double-error subspace which will be uncoupled from the logical one. It is spanned by the following states $\{|1100\rangle, |1010\rangle, |1001\rangle, |0110\rangle, |0101\rangle, |0011\rangle\}$. For a five-qubit repetition code, the number of such subspaces would amount to two and to three for a six-qubit one. It is straightforward to see that the number of equations in the permutation invariant system will thus scale as $N + 1$.

For $N = 4$, this system of equations looks like:

$$\frac{\mathrm{d}}{\mathrm{d}\tau}\begin{bmatrix} q \\ e \\ d \\ e^* \\ q^* \end{bmatrix} = \begin{bmatrix} -4i\omega - 4\Gamma_{\text{err}} & \Gamma_{\text{err}} + \Gamma_{\text{qec}} & 0 & 0 & 0 \\ 4\Gamma_{\text{err}} & -2i\omega - 4\Gamma_{\text{err}} - \Gamma_{\text{qec}} & \mathbf{2\Gamma}_{\text{err}} & 0 & 0 \\ 0 & 3\Gamma_{\text{err}} & -4\Gamma_{\text{err}} & 3\Gamma_{\text{err}} & 0 \\ 0 & 0 & \mathbf{2\Gamma}_{\text{err}} & 2i\omega - 4\Gamma_{\text{err}} - \Gamma_{\text{qec}} & 4\Gamma_{\text{err}} \\ 0 & 0 & 0 & \Gamma_{\text{err}} + \Gamma_{\text{qec}} & 4i\omega - 4\Gamma_{\text{err}} \end{bmatrix} \begin{bmatrix} q \\ e \\ d \\ e^* \\ q^* \end{bmatrix}, \tag{6.2}$$

where d represents the double errors subspace discussed above. As with the previously considered problem (cf. Eq. (3.8)), this system is convoluted and its solution is not trivial. Yet, one can simplify it using the same procedure as before, i.e. decouple the single errors subspaces e and e^* from the double ones by removing the orange terms from their equations. With this simplification, the system can be seamlessly solved. The eigenvalues are then: $\lambda_0 = -4\Gamma_{\text{err}}$, $\lambda_{1,2} = \lambda_\pm$ and $\lambda_{3,4} = \lambda_\pm^*$; with $\lambda_\pm$ being equal to:

$$\lambda_\pm = -\frac{1}{2}\,\Gamma_{\text{qec}} - 4\,\Gamma_{\text{err}} - 3i\omega \pm \frac{1}{2}\,\sqrt{D}\ . \tag{6.3}$$

The discriminant now has the following form:

$$D = \Gamma_{\text{qec}}^2 + 16\,\Gamma_{\text{qec}}\,\Gamma_{\text{err}} + 16\,\Gamma_{\text{err}}^2 - 4i\,\Gamma_{\text{qec}}\,\omega - 4\,\omega^2\ . \tag{6.4}$$

The eigenvectors are also similar to the previous ones such that the solution for the coherence $q(\tau)$ is given by approximately the same expression as its three qubit analogue derived in Eq. (4.6)

$$\begin{aligned} q(\tau) = &\left(\frac{\Gamma_{\text{qec}}}{4\sqrt{D}} - \frac{i\omega}{2\sqrt{D}} + \frac{1}{4}\right)\, \mathrm{e}^{\frac{1}{2}\tau\left(-\Gamma_{\text{qec}} - 8\Gamma_{\text{err}} - 6i\omega + \sqrt{D}\right)} \\ &- \left(\frac{\Gamma_{\text{qec}}}{4\sqrt{D}} - \frac{i\omega}{2\sqrt{D}} - \frac{1}{4}\right)\, \mathrm{e}^{\frac{1}{2}\tau\left(-\Gamma_{\text{qec}} - 8\Gamma_{\text{err}} - 6i\omega - \sqrt{D}\right)} \end{aligned} \tag{6.5}$$

We notice that the normalization constants did not change (cf. Eq. (4.7)) and only some numerical factors got altered which could be linked to the number of qubits in the system. The parity signal resulting from this expression naturally has a higher frequency due to the signal's Hamiltonian we considered (cf. Eq. (2.2)). Nonetheless, if we scale the sensing time as in Fig. 6.1, we see that the decay rate is also higher if the code is larger. Indeed, by increasing the size of the code words, we increase the number of possible decoherence channels and thus the overall probability of a decay event.

Using observations drawn from previous cases, we can now generalize the proposed solution to an arbitrary number of qubits $N \geq 3$. To construct the $(N+1)$x$(N+1)$ matrix for the permutation-invariant system of equations we have to follow some specific rules:

First, the error rates of each column should sum up to 0. Then, the diagonal elements should always be made of N decay channels ($-N\Gamma_{\text{err}}$ term) plus the evolution frequency in the given subspace. This frequency is easily determined from the states which span the subspace: if we look for instance at $|01011\rangle$, it is a member of the double-error subspace d for a five-qubit code word. As such, it evolves with only one ω because each 0 contributes $-\omega$ and each 1 $+\omega$. Finally, the upper diagonal of the matrix tells how many high-order errors could become lower-order errors. The decay happens at a rate equal to the number of erroneous qubits in this high order errors state (e.g. there exist only three possibilities to end up in a double-error subspace starting from triple-error one). Similarly, the lower diagonal expresses the opposite: how many low-order errors can become higher-order errors. This happens at a rate equal to the number of non-erroneous qubits in the low-order error state.

To be explicit, this matrix reads

$$\begin{bmatrix} -Ni\omega - N\Gamma_{\text{err}} & \Gamma_{\text{err}} + \Gamma_{\text{qec}} & 0 & 0 & \cdots \\ N\Gamma_{\text{err}} & -(N-2)i\omega - N\Gamma_{\text{err}} - \Gamma_{\text{qec}} & \mathbf{2\Gamma_{\text{err}}} & 0 & \cdots \\ 0 & (N-1)\Gamma_{\text{err}} & (N-4)i\omega - N\Gamma_{\text{err}} & 3\Gamma_{\text{err}} & \cdots \\ 0 & 0 & (N-3)\Gamma_{\text{err}} & (N-6)i\omega - N\Gamma_{\text{err}} & \cdots \\ \vdots & \vdots & \vdots & \vdots & \ddots \end{bmatrix} \tag{6.6}$$

where the first few components, denoted by $[\,q\,,\,e\,,\,d\,,t\,,\cdots]^{\text{T}}$, correspond to coherence and single, double and triple error subspaces respectively. As for Eq. (4.4) and Eq. (6.2), this system is convoluted due to the presence of QEC, but it can be simplified using the method explained in Section 4.2. It consists once again of removing the orange term from the matrix above. The spectrum of the simplified matrix has as members the terms $\lambda_\pm$ and $\lambda_\pm^*$ which are defined as:

$$\lambda_\pm = -\frac{1}{2}\,\Gamma_{\text{qec}} - N\,\Gamma_{\text{err}} - (N-1)i\omega \pm \frac{1}{2}\,\sqrt{D}\;, \tag{6.7}$$

with the discriminant:

$$D = \Gamma_{\text{qec}}^2 + 4N\,\Gamma_{\text{qec}}\,\Gamma_{\text{err}} + 4N\,\Gamma_{\text{err}}^2 - 4i\,\Gamma_{\text{qec}}\,\omega - 4\,\omega^2 \tag{6.8}$$

We find that the solution for the coherence is given by the following function.

$$\begin{aligned} q(\tau) = &\left(\frac{\Gamma_{\text{qec}}}{4\sqrt{D}} - \frac{i\omega}{2\sqrt{D}} + \frac{1}{4}\right)\,\mathrm{e}^{\,\frac{1}{2}\tau\left(-\Gamma_{\text{qec}} - 2N\Gamma_{\text{err}} - 2(N-1)i\omega + \sqrt{D}\right)} \\ &- \left(\frac{\Gamma_{\text{qec}}}{4\sqrt{D}} - \frac{i\omega}{2\sqrt{D}} - \frac{1}{4}\right)\,\mathrm{e}^{\,\frac{1}{2}\tau\left(-\Gamma_{\text{qec}} - 2N\Gamma_{\text{err}} - 2(N-1)i\omega - \sqrt{D}\right)}\;. \end{aligned} \tag{6.9}$$

As for the four-qubit code, we note that the normalization terms remain unchanged and the numerical factors are now dependent on the number of qubits N.

For this generalized repetition code, we can derive the reduced solution, as we performed it in Section 4.3 for the three-qubit case. The validity of this expression will be imposed by the same two inequalities (cf. Eq. (4.10)) except that the factor 12 will be substituted by $4N$. The reduced form of the parity function is then

$$\mathbb{P}_1(\tau) = \frac{1}{2} + \frac{1}{2}\,\mathrm{e}^{-N\,\Gamma_{\text{eff}}\,\tau}\,\cos[\,N\,\omega_{\text{eff}}\,\tau\,] \tag{6.10}$$

with the following effective parameters

$$\begin{aligned}\omega_{\text{eff}} &= \omega\left(1 - 2\,\frac{\Gamma_{\text{err}}}{\Gamma_{\text{qec}}}\right) \ , \\ \Gamma_{\text{eff}} &= (N-1)\,\frac{\Gamma_{\text{err}}}{\Gamma_{\text{qec}}}\Gamma_{\text{err}} \ .\end{aligned} \tag{6.11}$$

It is important to note that the total decay rate and frequency are not merely increasing with the number of qubits N, but that this increase is quadratic for the former and only linear for the latter. This confirms our previous observation about Fig. 6.1. Furthermore, if we wanted to keep the contrast of the Ramsey fringes constant while increasing the number of two level systems, we would need to increase the correction rate linearly with $(N-1)$ which would consequently result in a linear reduction of the frequency bias.

6.2. Two-qubit sensing protocol

Let us now look at the special two qubit case. Unlike an N-qubit repetition code, it does not have any double-error subspace and the single-error subspaces overlap with each other, since $|01\rangle$ is an erroneous state of $|00\rangle$ and, at the same time, of $|11\rangle$. In order to use such a system for quantum sensing, we must assume that one of the qubits has a much larger coherence time than the other one. This type of encoding is not a novelty and has already been previously studied [19, 21, 27, 48, 49]. Here we consider states $|\psi_{\text{s}}\rangle \otimes |\psi_{\text{p}}\rangle$ where s and p indicate the sensing and protection qubits respectively, such that $\Gamma_{\text{err}}^{(\text{s})} \gg \Gamma_{\text{err}}^{(\text{p})}$. This could be achieved using for instance two different species of ions in a trapped ion setup. When considering a situation like this, one has to distinguish as

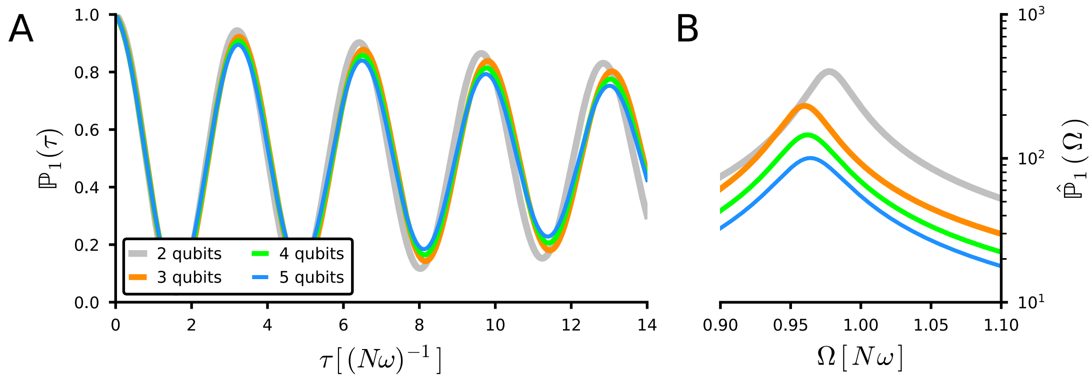

Figure 6.1.: *Parity signal for larger codes.* **A.** Ramsey signal for various sizes N of repetition codes. It was obtained with the formula $\mathbb{P}_1(\tau) = 1/2 + \text{Re}(q(\tau))$ where the coherence $q(\tau)$ is given in Eq. (6.9). The only exception is the two qubit case where we use Eq. (6.14). **B.** Discrete Fourier transform of the signals from **A.**

well the transition energies of the qubits, i.e. $\omega^{(\mathrm{s})} \neq \omega^{(\mathrm{p})}$. The system has then only one QEC jump operator given by the following expression,

$$L_{\mathrm{qec}}^{(\mathrm{s})} = \sqrt{\Gamma_{\mathrm{qec}}}\,\sigma_x^{(\mathrm{s})}\,\frac{1-\sigma_z^{(\mathrm{s})}\,\sigma_z^{(\mathrm{p})}}{2}\ .$$

The full matrix differential equation describing the dynamics is given by

$$\begin{bmatrix} \begin{array}{c}-i\,(\omega^{(\mathrm{p})}+\omega^{(\mathrm{s})})-\\ -\,(\Gamma_{\mathrm{err}}^{(\mathrm{s})}+\Gamma_{\mathrm{err}}^{(\mathrm{p})})\end{array} & \Gamma_{\mathrm{err}}^{(\mathrm{s})}+\Gamma_{\mathrm{qec}} & \boldsymbol{\Gamma}_{\mathrm{err}}^{(\mathrm{p})} & 0 \\ \Gamma_{\mathrm{err}}^{(\mathrm{s})} & \begin{array}{c}-i\,(\omega^{(\mathrm{p})}-\omega^{(\mathrm{s})})-\\ -\,(\Gamma_{\mathrm{err}}^{(\mathrm{s})}+\Gamma_{\mathrm{err}}^{(\mathrm{p})}+\Gamma_{\mathrm{qec}})\end{array} & 0 & \boldsymbol{\Gamma}_{\mathrm{err}}^{(\mathrm{p})} \\ \boldsymbol{\Gamma}_{\mathrm{err}}^{(\mathrm{p})} & 0 & \begin{array}{c}i\,(\omega^{(\mathrm{p})}-\omega^{(\mathrm{s})})-\\ -\,(\Gamma_{\mathrm{err}}^{(\mathrm{s})}+\Gamma_{\mathrm{err}}^{(\mathrm{p})}+\Gamma_{\mathrm{qec}})\end{array} & \Gamma_{\mathrm{err}}^{(\mathrm{s})} \\ 0 & \boldsymbol{\Gamma}_{\mathrm{err}}^{(\mathrm{p})} & \Gamma_{\mathrm{err}}^{(\mathrm{s})}+\Gamma_{\mathrm{qec}} & \begin{array}{c}i\,(\omega^{(\mathrm{p})}+\omega^{(\mathrm{s})})-\\ -\,(\Gamma_{\mathrm{err}}^{(\mathrm{s})}+\Gamma_{\mathrm{err}}^{(\mathrm{p})})\end{array} \end{bmatrix},$$

where the components are $[\,q\,,\,e\,,\,e^*\,,q^*\,]^{\mathrm{T}}$. To be explicit, the coherence term is equal to $q = \langle 11|\,\rho\,|00\rangle$ and the erroneous one to $e = \langle 01|\,\rho\,|10\rangle$. Here, as in all the previous cases, to solve the problem we simplify the matrix by removing selected terms. However, due to the small number of qubits this has to be done in two places (see the orange elements in the matrix). The logic behind this operation remains the same, though: decoupling the upper block (q, e) of the matrix from the lower one (e^*, q^*). Then it becomes block diagonal and seamlessly solvable. The four eigenvalues are $\lambda_\pm$ and $\lambda_\pm^*$ are determined as

$$\lambda_\pm = -\frac{1}{2}\,\Gamma_{\mathrm{qec}} - (\Gamma_{\mathrm{err}}^{(\mathrm{s})}+\Gamma_{\mathrm{err}}^{(\mathrm{p})}) - i\omega^{(\mathrm{p})} \pm \sqrt{D}\ , \tag{6.12}$$

with discriminants:

$$D = \Gamma_{\mathrm{qec}}^2 + 4\,\Gamma_{\mathrm{qec}}\,\Gamma_{\mathrm{err}}^{(\mathrm{s})} + 4\,\Gamma_{\mathrm{err}}^{(\mathrm{s})\,2} - 4i\,\Gamma_{\mathrm{qec}}\,\omega^{(\mathrm{s})} - 4\,\omega^{(\mathrm{s})\,2}\ . \tag{6.13}$$

The solution for the coherence $q(\tau)$ is then derived from the initial-value problem and is equal to:

$$\begin{aligned} q(\tau) = &\left(\frac{\Gamma_{\mathrm{qec}}}{4\sqrt{D}} - \frac{i\omega^{(\mathrm{s})}}{2\sqrt{D}} + \frac{1}{4}\right)\,\mathrm{e}^{\,\frac{1}{2}\tau\left(-\Gamma_{\mathrm{qec}}-2(\Gamma_{\mathrm{err}}^{(\mathrm{s})}+\Gamma_{\mathrm{err}}^{(\mathrm{p})})-2i\omega^{(\mathrm{p})}+\sqrt{D}\right)} \\ &-\left(\frac{\Gamma_{\mathrm{qec}}}{4\sqrt{D}} - \frac{i\omega^{(\mathrm{s})}}{2\sqrt{D}} - \frac{1}{4}\right)\,\mathrm{e}^{\,\frac{1}{2}\tau\left(-\Gamma_{\mathrm{qec}}-2(\Gamma_{\mathrm{err}}^{(\mathrm{s})}+\Gamma_{\mathrm{err}}^{(\mathrm{p})})-2i\omega^{(\mathrm{p})}-\sqrt{D}\right)}\ . \end{aligned} \tag{6.14}$$

As expected, only the sensing qubit contributes to the frequency bias. We can see that from the discriminant which has no dependence on $\omega^{(\mathrm{p})}$. It is even more obvious when we consider the reduced solution,

$$\mathbb{P}_1(\tau) = \frac{1}{2} + \frac{1}{2}\,\mathrm{e}^{-\Gamma_{\mathrm{err}}^{(\mathrm{p})}\,\tau} \cos\left[\left(\omega^{(\mathrm{p})} + \omega^{(\mathrm{s})} - 2\,\frac{\Gamma_{\mathrm{err}}^{(\mathrm{s})}}{\Gamma_{\mathrm{qec}}}\right)\tau\right] . \tag{6.15}$$

This equation also shows that the sensing qubit does not impact the decay rate, at least in the scope of this approximation which is still given by inequalities (4.10)[i].

Fig. 6.1 shows the Ramsey signal obtained using such an encoding. For the observed comparison, the frequencies of the qubits were both set to 1. We can observe that signal agrees with our conclusion from above: it has a better contrast and its bias increases slower compared to the other encodings with the same correction rate Γ_{qec}.

[i]Except that all Γ_{err} must be replaced by $\Gamma_{\mathrm{err}}^{(\mathrm{s})}$ and the factor of 12 by only 4.

Chapter 7

Conclusion & Outlook

In this thesis, I exposed the emergence of a systematic bias in an error-corrected quantum sensing protocol and presented a theoretical explanation for it. The analysis was performed from a purely quantum information perspective.

I started by broadly presenting the principles of quantum sensing and the main challenges behind the usage of quantum error correction (QEC). The Ramsey sequence was my choice of sensing protocol for illustrating the bias. The sequence in the presence of dissipative decoherence and QEC was analytically solved for non-corrected, as well as corrected systems. Even though the latter needed a simplification, both solutions showed a good agreement with the simulations and a deviation from a standard expected formula. An approximation of these results exposed the origin of the bias and reduced the equations to a more useful form. Finally, in the last two chapters, I presented various analyses of the derived solutions, exposed consequences of the bias, and generalizations to other types of repetition codes.

This work can be ultimately completed by engineering a method to compensate the bias throughout the course of the sensing protocol. A first step towards this direction was proposed in the Section 5.6 where I presented an adaptive sensing protocol. The main challenge for this method is to answer to question: how to correct the bias with no prior knowledge of the true frequency ω?

Another interesting outlook is to consider other types of encoding, rather than the simple repetition codes studied in this work, with the aim of finding a bias-proof code which would not need any compensation of the frequency. This could be achieved by designing codewords for which the evolution frequency is the same in the logical and erroneous subspaces.

Furthermore, one can as well investigate the correction of higher-order errors in repetition codes which could eventually lead to fault tolerance in quantum sensing and quantum computation.

Proposed solution vs Simulation

An aspect not discussed in the main text is the precision of the proposed solution with respect to a simulation of the protocol. Fig. A.1A shows the root-mean-square deviation (RMSE) of the parity function given in Eq. (4.8) from the Ramsey signal simulated with QuTiP [41]. We note that the error is consistently below 0.2% indicating that the function is an equally accurate solution of the non-corrected and error-corrected problems. We believe that this error is due to the assumption that we had to make to solve the problem in the first place (cf. Section 4.2).

Furthermore, Fig. A.1 displays as well the RMSE of the proposed sensitivity formula presented in Eq. (5.14) with respect to its simulation. Notwithstanding some discrepancies for high correction rates, the baseline of the error curve depicts a very fast decrease and crosses the cap of 1% already for low Γ_{qec}. The variations mentioned previously as well as the trend of the error curve when $\Gamma_{\text{qec}} \to 0$ could come from discretization errors. Indeed, for the simulated data, we approximated the derivative $\partial_\omega \mathbb{P}_1(\tau)$ with a finite difference method such that these errors could potentially be reduced with a finer frequency discretization or a higher order method.

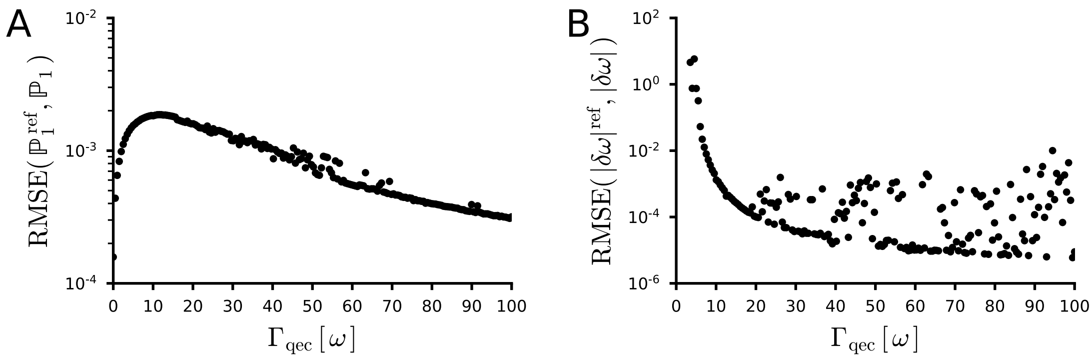

Figure A.1.: *Error between the simulation and the proposed functions.* The root-mean-square error (RMSE) calculated as in Eq. (5.2) between the analytically derived expressions and their simulations obtained with QuTiP. These expressions are (A) the proposed parity function (cf. Eq. (4.8)), (B) the sensitivity formula (cf. Eq. (5.14)).

Appendix B

Convergence of the reduced parity function

In Section 4.3, we approximate the full expression of an error-corrected Ramsey signal given in Eq. (4.8) with a much simpler and closer to the standard form function. The latter, presented in Eq. (4.11), was derived by expanding the square root of the discriminant D (cf. Eq. (4.9)) and considering only the first order terms in $\mathcal{O}(1/\Gamma_{\mathrm{qec}})$. This implies that the effective parameters, stated in Eq. (4.12), are as well first-order approximations of the true decay rate and frequency of the signal which, as we show it in Fig. 5.6, causes a deviation of the approximated sensitivity from the true one.

However, this can be improved by refining the expression of ω_{eff} and Γ_{eff}. The next two approximation orders are the following:

$$
\begin{aligned}
\omega_{\mathrm{eff}} &= \omega\left(1 \underbrace{-\,2\,\frac{\Gamma_{\mathrm{err}}}{\Gamma_{\mathrm{qec}}}}_{\text{1st order}} \underbrace{+\,16\,\frac{\Gamma_{\mathrm{err}}^2}{\Gamma_{\mathrm{qec}}^2}}_{\text{2nd order}} \underbrace{-\,141\,\frac{\Gamma_{\mathrm{err}}^3}{\Gamma_{\mathrm{qec}}^3} + 8\,\frac{\Gamma_{\mathrm{err}}\,\omega^2}{\Gamma_{\mathrm{qec}}^3}}_{\text{3rd order}}\right) \\
\Gamma_{\mathrm{eff}} &= \underbrace{2\,\frac{\Gamma_{\mathrm{err}}}{\Gamma_{\mathrm{qec}}}\Gamma_{\mathrm{err}}}_{\text{1st order}} \underbrace{-\,12\,\frac{\Gamma_{\mathrm{err}}^2}{\Gamma_{\mathrm{qec}}^2}\Gamma_{\mathrm{err}} + 4\,\frac{\omega^2}{\Gamma_{\mathrm{qec}}^2}\Gamma_{\mathrm{err}}}_{\text{2nd order}} \underbrace{+\,84\,\frac{\Gamma_{\mathrm{err}}^3}{\Gamma_{\mathrm{qec}}^3}\Gamma_{\mathrm{err}} - 68\,\frac{\Gamma_{\mathrm{err}}\,\omega^2}{\Gamma_{\mathrm{qec}}^3}\Gamma_{\mathrm{err}}}_{\text{3rd order}}
\end{aligned}
\tag{B.1}
$$

We see that the effective decay rate now has a dependence on the true frequency ω as well. To study the precision of these approximations, one can measure the root-mean-square deviation (cf. Eq. (5.2)) of the resulting parity functions with respect to the proposed one[i]. Fig. B.1A illustrates this quantity as a function of the correction rate Γ_{qec}. The plot shows that the error between both functions is, in the scope of the validity range, below 10% and for the 2nd and 3rd order approximations it even becomes very quickly of the magnitude of 0.1%. The same measure can be done on with sensitivities as depicted in Fig. B.1B. Here, the approximated sensitivities, calculated with Eq. (5.15), were compared to the full expression given in Eq. (5.14). Unlike in the previous case, for low Γ_{qec}, the sensitivity is better approximated by the 1st and 3rd order expressions of the effective parameters than by the 2nd order one. All of them nevertheless converge relatively quickly to a same value below 1%.

[i]We do not compare these functions to their simulated counterparts as in Appendix A, because their calculation is highly resource demanding.

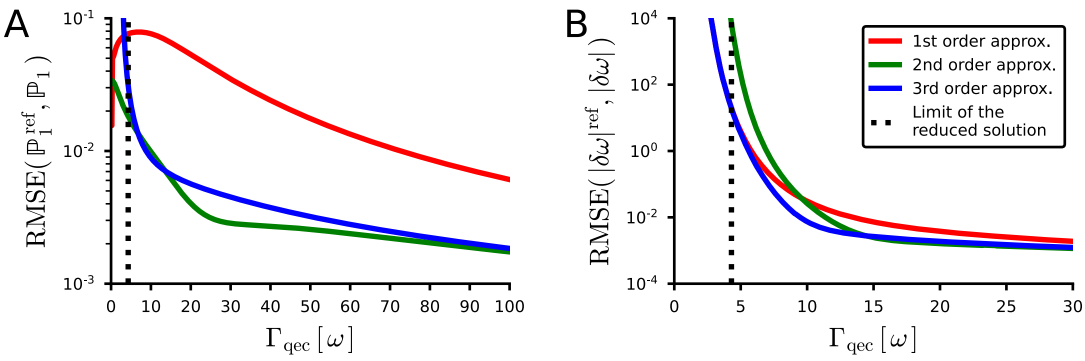

Figure B.1.: *Error between the proposed solution and its approximation.* The root-mean-square error (RMSE) calculated as in Eq. (5.2) between: (A) the proposed parity function (cf. Eq. (4.8)) and its reduced form (cf. Eq. (4.11)); (B) the sensitivity (cf. Eq. (5.14)) and its approximation (cf. Eq. (5.15)). The curves differ in the order of approximation of the effective parameters as presented in Eq. (B.1).

The last observation suggests that the high error of the 1st order approximation in Fig. B.1A originates from a poor approximation of the exponential decay rather than the oscillations' frequency. We can confirm this hypothesis by investigating the deviation of ω_{eff} as stated in Eq. (B.1) from the true effective frequency obtained using a discrete Fourier transform of the proposed parity function. Fig. B.2 shows how the absolute value of this quantity changes with Γ_{qec}. Since for all orders the error is below 1% and converges quickly to lower values, it constitutes an equivocal evidence of the proof of the hypothesis, that the major part of the error comes from a loose approximation of Γ_{eff}.

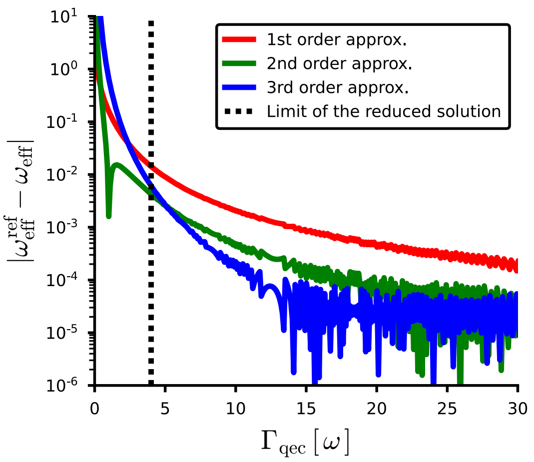

Figure B.2: *Error of the effective frequency.* Absolute deviation of the approximated effective frequency stated in Eq. (B.1) from its true value, obtained using a discrete Fourier transform of the proposed parity function (cf. Eq. (4.8)).

Bibliography

[1] H. Hertz, "Ueber einen einfluss des ultravioletten lichtes auf die electrische entladung", Ann. Phys. **267**, 983–1000 (1887).

[2] W. Gerlach and O. Stern, "Der experimentelle Nachweis der Richtungsquantelung im Magnetfeld", Zeitschrift für Physik **9**, 349–352 (1922).

[3] V. Giovannetti, S. Lloyd, and L. Maccone, "Quantum-enhanced measurements: beating the standard quantum limit", Science **306**, 1330–1336 (2004).

[4] V. Giovannetti, S. Lloyd, and L. Maccone, "Quantum metrology", Phys. Rev. Lett. **96**, 010401 (2006).

[5] V. Giovannetti, S. Lloyd, and L. Maccone, "Advances in quantum metrology", Nat. Photonics **5**, 222–229 (2011).

[6] M. Tse et al., "Quantum-enhanced advanced LIGO detectors in the era of gravitational-wave astronomy", Phys. Rev. Lett. **123**, 231107 (2019).

[7] C. L. Degen, F. Reinhard, and P. Cappellaro, "Quantum sensing", Rev. Mod. Phys. **89**, 035002 (2017).

[8] M. A. Nielsen and I. L. Chuang, *Quantum computation and quantum information: 10th anniversary edition* (Cambridge University Press, Cambridge, 2010).

[9] P. W. Shor, "Scheme for reducing decoherence in quantum computer memory", Phys. Rev. A **52**, R2493–R2496 (1995).

[10] A. M. Steane, "Error correcting codes in quantum theory", Phys. Rev. Lett. **77**, 793–797 (1996).

[11] D. Layden, "Device- and application-adapted quantum error correction", PhD thesis (Massachusetts Institute of Technology, 2020).

[12] M. J. Biercuk, H. Uys, A. P. VanDevender, N. Shiga, W. M. Itano, and J. J. Bollinger, "Optimized dynamical decoupling in a model quantum memory", Nature **458**, 996–1000 (2009).

[13] W. M. Witzel, M. S. Carroll, A. Morello, \. Cywiński, and S. Das Sarma, "Electron spin decoherence in isotope-enriched silicon", Phys. Rev. Lett. **105**, 187602 (2010).

[14] H. Bluhm, S. Foletti, I. Neder, M. Rudner, D. Mahalu, V. Umansky, and A. Yacoby, "Dephasing time of GaAs electron-spin qubits coupled to a nuclear bath exceeding 200 mu s", Nat. Phys. **7**, 109–113 (2011).

[15] J. T. Muhonen, J. P. Dehollain, A. Laucht, F. E. Hudson, R. Kalra, T. Sekiguchi, K. M. Itoh, D. N. Jamieson, J. C. McCallum, A. S. Dzurak, and A. Morello, "Storing quantum information for 30 seconds in a nanoelectronic device", Nat. Nanotechnol. **9**, 986–991 (2014).

[16] J.-L. Orgiazzi, C. Deng, D. Layden, R. Marchildon, F. Kitapli, F. Shen, M. Bal, F. R. Ong, and A. Lupascu, "Flux qubits in a planar circuit quantum electrodynamics architecture: quantum control and decoherence", Phys. Rev. B **93**, 104518 (2016).

[17] T. Kobayashi, J. Salfi, C. Chua, J. van der Heijden, M. G. House, D. Culcer, W. D. Hutchison, B. C. Johnson, J. C. McCallum, H. Riemann, N. V. Abrosimov, P. Becker, H.-J. Pohl, M. Y. Simmons, and S. Rogge, "Engineering long spin coherence times of spin–orbit qubits in silicon", Nat. Mater., 1–5 (2020).

[18] R. Ozeri, "Heisenberg limited metrology using quantum error-correction codes", arXiv:1310.3432 [quant-ph] (2013).

[19] E. M. Kessler, I. Lovchinsky, A. O. Sushkov, and M. D. Lukin, "Quantum error correction for metrology", Phys. Rev. Lett. **112**, 150802 (2014).

[20] W. Dür, M. Skotiniotis, F. Fröwis, and B. Kraus, "Improved quantum metrology using quantum error correction", Phys. Rev. Lett. **112**, 080801 (2014).

[21] G. Arrad, Y. Vinkler, D. Aharonov, and A. Retzker, "Increasing sensing resolution with error correction", Phys. Rev. Lett. **112**, 150801 (2014).

[22] D. A. Herrera-Martí, T. Gefen, D. Aharonov, N. Katz, and A. Retzker, "Quantum error-correction-enhanced magnetometer overcoming the limit imposed by relaxation", Phys. Rev. Lett. **115**, 200501 (2015).

[23] M. B. Plenio and S. F. Huelga, "Sensing in the presence of an observed environment", Phys. Rev. A **93**, 032123 (2016).

[24] T. Gefen, D. A. Herrera-Martí, and A. Retzker, "Parameter estimation with efficient photodetectors", Phys. Rev. A **93**, 032133 (2016).

[25] F. Reiter, A. S. Sørensen, P. Zoller, and C. A. Muschik, "Dissipative quantum error correction and application to quantum sensing with trapped ions", Nat. Commun. **8**, 1822 (2017).

[26] Y. Matsuzaki and S. Benjamin, "Magnetic-field sensing with quantum error detection under the effect of energy relaxation", Phys. Rev. A **95**, 032303 (2017).

[27] T. Unden, P. Balasubramanian, D. Louzon, Y. Vinkler, M. B. Plenio, M. Markham, D. Twitchen, A. Stacey, I. Lovchinsky, A. O. Sushkov, M. D. Lukin, A. Retzker, B. Naydenov, L. P. McGuinness, and F. Jelezko, "Quantum metrology enhanced by repetitive quantum error correction", Phys. Rev. Lett. **116**, 230502 (2016).

[28] L. Cohen, Y. Pilnyak, D. Istrati, A. Retzker, and H. S. Eisenberg, "Demonstration of a quantum error correction for enhanced sensitivity of photonic measurements", Phys. Rev. A **94**, 012324 (2016).

[29] L. Viola and S. Lloyd, "Dynamical suppression of decoherence in two-state quantum systems", Phys. Rev. A **58**, 2733–2744 (1998).

[30] J. M. Taylor, P. Cappellaro, L. Childress, L. Jiang, D. Budker, P. R. Hemmer, A. Yacoby, R. Walsworth, and M. D. Lukin, "High-sensitivity diamond magnetometer with nanoscale resolution", Nat. Phys. **4**, 810–816 (2008).

[31] J.-M. Cai, B. Naydenov, R. Pfeiffer, L. P. McGuinness, K. D. Jahnke, F. Jelezko, M. B. Plenio, and A. Retzker, "Robust dynamical decoupling with concatenated continuous driving", New J. Phys. **14**, 113023 (2012).

[32] J. E. Lang, R. B. Liu, and T. S. Monteiro, "Dynamical-decoupling-based quantum sensing: floquet spectroscopy", Phys. Rev. X **5**, 041016 (2015).

[33] A. Lazariev, S. Arroyo-Camejo, G. Rahane, V. K. Kavatamane, and G. Balasubramanian, "Dynamical sensitivity control of a single-spin quantum sensor", Sci. Rep. **7**, 6586 (2017).

[34] S. Schmitt, T. Gefen, F. M. Stürner, T. Unden, G. Wolff, C. Müller, J. Scheuer, B. Naydenov, M. Markham, S. Pezzagna, J. Meijer, I. Schwarz, M. Plenio, A. Retzker, L. P. McGuinness, and F. Jelezko, "Submillihertz magnetic spectroscopy performed with a nanoscale quantum sensor", Science **356**, 832–837 (2017).

[35] G. T. Genov, N. Aharon, F. Jelezko, and A. Retzker, "Mixed dynamical decoupling", Quantum Science and Technology **4**, 035010 (2019).

[36] M. Ban, "Photon-echo technique for reducing the decoherence of a quantum bit", J. Mod. Opt. **45**, 2315–2325 (1998).

[37] D. Layden and P. Cappellaro, "Spatial noise filtering through error correction for quantum sensing", npj Quantum Inf. **4**, 1–6 (2018).

[38] H. Breuer, P. Breuer, F. Petruccione, and S. Petruccione, *The theory of open quantum systems* (Oxford University Press, 2002).

[39] N. F. Ramsey, "A molecular beam resonance method with separated oscillating fields", Phys. Rev. **78**, 695–699 (1950).

[40] S. F. Huelga, C. Macchiavello, T. Pellizzari, A. K. Ekert, M. B. Plenio, and J. I. Cirac, "Improvement of frequency standards with quantum entanglement", Phys. Rev. Lett. **79**, 3865–3868 (1997).

[41] J. R. Johansson, P. D. Nation, and F. Nori, "QuTiP 2: a python framework for the dynamics of open quantum systems", Comput. Phys. Commun. **184**, 1234 –1240 (2013).

[42] I. T. Jolliffe and J. Cadima, "Principal component analysis: a review and recent developments", Philosophical Transactions of the Royal Society A: Mathematical, Physical and Engineering Sciences **374**, 20150202 (2016).

[43] C. R. Harris et al., "Array programming with NumPy", Nature **585**, 357–362 (2020).

[44] H. Cramér, *Mathematical methods of statistics (PMS-9)* (Princeton University Press, 1999).

[45] C. W. Helstrom, *Quantum detection and estimation theory*, Math. Sci. Eng 123 (Academic Press, New York, NY, 1976).

[46] J. Liu, H. Yuan, X.-M. Lu, and X. Wang, "Quantum fisher information matrix and multiparameter estimation", J. Phys. A: Math. Theor. **53**, 023001 (2019).

[47] S. Geman, E. Bienenstock, and R. Doursat, "Neural networks and the bias/variance dilemma.", Neural Comput. **4**, 1–58 (1992).

[48] R. Demkowicz-Dobrzański, J. Czajkowski, and P. Sekatski, "Adaptive quantum metrology under general markovian noise", Phys. Rev. X **7**, 041009 (2017).

[49] S. Zhou, M. Zhang, J. Preskill, and L. Jiang, "Achieving the heisenberg limit in quantum metrology using quantum error correction", Nat. Commun. **9**, 78 (2018).

Eidgenössische Technische Hochschule Zürich
Swiss Federal Institute of Technology Zurich

Declaration of originality

The signed declaration of originality is a component of every semester paper, Bachelor's thesis, Master's thesis and any other degree paper undertaken during the course of studies, including the respective electronic versions.

Lecturers may also require a declaration of originality for other written papers compiled for their courses.

I hereby confirm that I am the sole author of the written work here enclosed and that I have compiled it in my own words. Parts excepted are corrections of form and content by the supervisor.

Title of work (in block letters):

Bias in error-corrected quantum sensing

Authored by (in block letters):
For papers written by groups the names of all authors are required.

Name(s):	First name(s):
Rojkov	Ivan

With my signature I confirm that
- I have committed none of the forms of plagiarism described in the 'Citation etiquette' information sheet.
- I have documented all methods, data and processes truthfully.
- I have not manipulated any data.
- I have mentioned all persons who were significant facilitators of the work.

I am aware that the work may be screened electronically for plagiarism.

Place, date
Zürich, 07.12.2020

Signature(s)

For papers written by groups the names of all authors are required. Their signatures collectively guarantee the entire content of the written paper.